Nature Communications

https://doi.org/10.1038/s41467-026-69720-6

Article in Press

Post-treatment SIV control is associated with specific features of viral persistence before and after treatment interruption

Received: 19 June 2025

Accepted: 6 February 2026

Cite this article as: Charre, C., Melard, A., Chaillon, A. *et al.* Post-treatment SIV control is associated with specific features of viral persistence before and after treatment interruption. *Nat Commun* (2026). https://doi.org/10.1038/s41467-026-69720-6

Caroline Charre, Adeline Melard, Antoine Chaillon, Elise Gardiennet, Delphine Desjardins, Caroline Passaes, Antoine Millet, Marine Fillion, Nastasia Dimant, Valérie Monceaux, Nathalie Dereuddre-Bosquet, Olivier Lambotte, Michaela Muller-Trutwin, Christine Rouzioux, Roger Le Grand, Asier Saez- Cirion & Véronique Avettand-Fenoel

Post-treatment SIV control is associated with specific features of viral persistence before and after treatment interruption

Caroline CHARRE[1,2#], Adeline MELARD[1], Antoine CHAILLON[3], Elise GARDIENNET[1], Delphine DESJARDINS[4], Caroline PASSAES[5,6], Antoine MILLET[1], Marine FILLION[1], Nastasia DIMANT[4], Valérie MONCEAUX[5,6], Nathalie DEREUDDRE-BOSQUET[4], Olivier LAMBOTTE[4,7], Michaela MULLER-TRUTWIN[6], Christine ROUZIOUX[8], Roger LE GRAND[4], Asier SAEZ- CIRION[5,6], Véronique AVETTAND-FENOEL[1,9,10#]

[1] Université Paris Cité, INSERM, U1016; CNRS, UMR8104 Paris, France

[2] AP-HP, Hôpital Cochin, Service de Virologie, Paris, France

[3] University of California, Department of Medicine/Division of Infectious Diseases, San Diego, United States

[4] Université Paris-Saclay, CEA, INSERM, UMR1184, Immunology of Viral Auto-immune, Hematological and Bacterial diseases (IMVA-HB/ IDMIT Department), Fontenay-aux-Roses/Le Kremlin-Bicêtre, France.

[5] Institut Pasteur, Université Paris Cité, Viral Reservoirs and Immune Control Unit, Paris, France.

[6] Institut Pasteur, Université Paris Cité, HIV Inflammation and Persistence Unit, Paris, France.

[7] Université Paris-Saclay, AP-HP. Hôpital Bicêtre, Clinical Immunology Department, Le Kremlin Bicêtre, France.

[8] Université Paris Cité, Paris, France.

[9] CHU d'Orléans, Orléans, France.

[10] Université d'Orléans, LI2RSO, Orléans, France.

Corresponding authors: Véronique AVETTAND-FENOEL, veronique.avettand-fenoel@chu-orleans.fr; Caroline CHARRE, caroline.charre@aphp.fr

Abstract

Mechanisms underlying durable control of HIV after antiretroviral therapy interruption remain poorly understood. Here we provide a comprehensive longitudinal analysis in a non-human primate model of post-treatment control using SIVmac251-infected male cynomolgus macaques (pVISCONTI study). Controllers exhibit lower levels of SIV DNA, intact proviruses, transcriptional activity, and viral evolution compared to non-controllers in blood and tissues long after therapy interruption. Before interruption, controllers already have fewer intact proviruses in lymph nodes, and this difference persists in blood shortly after interruption, prior to viral rebound. Intact provirus levels in lymph nodes before interruption negatively correlate with $CD8^+$ T-cell capacity to suppress SIV and reflect rebound magnitude. The study demonstrates that markers of post-treatment control are detectable in lymph nodes before therapy interruption and in blood shortly after, and suggests that host immune responses may shape intact provirus profiles during treatment.

Introduction

The persistence of HIV genome integrated into the host genome, forming proviruses, is the main obstacle to HIV cure. The infected cells harboring proviruses are distributed across various anatomical sites, forming reservoirs[1]. While antiretroviral treatment (ART) can help maintain undetectable plasma viral loads, it falls short of eliminating HIV reservoirs. Upon discontinuation of ART, most persons living with HIV (PLWH) experience rapid viral rebound[2–4], thought to mainly come from memory CD4+T cells containing genetically intact proviruses[5–13]. However, a specific sub-group of PLWH who are most often treated early after infection and are referred as post-

treatment controllers (PTCs), exhibit prolonged suppression of viremia after ART discontinuation[14–16]. The landmark VISCONTI study[15], confirmed afterward by the CHAMP study[17] and supported by mathematical modeling of latent viral reservoir dynamics[18] and macaque models[19,20], is the proof of concept that initiating ART within the first weeks after infection and maintaining it for several years favors post-treatment control (PTC). This can be related to multiple non-mutually exclusive factors, including the significant reduction of HIV reservoirs following early treatment[21]. However, initiating ART too soon after infection gave disappointing results[22], as if a minimal period of exposure to the viral antigen was necessary for the development of a better immune response to maintain PTC. Moreover, early initiation of treatment after infection is insufficient to explain post-treatment control, as only a small proportion of early treated PLWH are becoming PTCs[15–17]. Thus, efforts to identify underlying mechanisms driving PTC and predictive biomarkers are essential for developing such HIV remission strategies. While viral and immunological biomarkers such as low HIV DNA levels in blood or high CD4/CD8 ratios are commonly found in PTCs[23–26], these features alone do not reliably predict sustained control, and the specific mechanisms by which HIV control is maintained after interrupting ART are not clearly understood. Heterogeneity in time to ART initiation, ART regimens, duration of ART prior to interruption, genetic and environmental diversity, as well as the criteria employed to define PTCs in diverse human cohorts pose challenges in gaining a comprehensive understanding of the PTC[14,25]. Additionally, except rare studies[27–32], occasionally conducted in PLWH after autopsy[28,29,31,32], the comprehensive investigation of HIV reservoirs in deep tissues is complicated. Most studies aimed at understanding HIV reservoirs in PTCs have primarily focused on blood[14] and only few on profound tissues[27]. Yet, considering that circulating CD4+ T lymphocytes in the blood constitute only 2% of

whole-body CD4+ T lymphocytes[33] and most infected cells persist in tissues[31,34–37], the analysis of deep tissue reservoirs would undoubtedly offer significant additional information to clarify underlying mechanisms of PTC. To address these challenges, SIV infection of nonhuman primates (NHP) reproduces events following HIV infection in human[19,38–41] and provide an opportunity to investigate deep tissue reservoir seeding by extensive tissue sampling. The p(rimate)VISCONTI project has consisted in investigating the impact of early initiation of ART on the development of PTC status in cynomolgus macaques (CyMs) infected with SIVmac251, in standardized experimental conditions (Fig 1a). First results of the pVISCONTI project[19] confirmed that initiating ART during the early stage of infection, at week 4 (W4) vs W24 post-infection (pi) significantly enhanced SIV PTC. Specifically, 9 out of 11 macaques treated early developed PTC status with plasma viral loads dropping below 400 copies/mL, either directly or after a transient rebound, and remaining low during the 6-month follow-up after ATI. In contrast, only 2 macaques of 11 treated later at 24 weeks (W24) pi achieved similar outcomes, as most lost virological control after ATI (Fig. S1b-e). Additionally, this study showed that 2 years of ART initiated early after infection was associated with the establishment of a pool of memory CD8+ T cells with enhanced antiviral potential after ATI. Thus, allowing immune response maturation might be crucial for controlling the virus after ATI[19,42]. Here, we aimed to investigate whether intrinsic viral characteristics of SIV persistence in blood and deep tissues were associated with PTC. We extensively analyzed SIV reservoirs in PTCs and non controllers (NCs) of the pVISCONTI study, longitudinally in blood and peripheral lymph nodes (PLN) specimens and in blood and tissues from 40 anatomical sites at euthanasia. We demonstrated that the PTC status was associated with a prolonged restriction of reservoirs several months after ATI in terms of estimated size, transcriptional activity, proviral evolution and intactness in the blood and various tissues. A small

pool of intact proviruses in PLN before ATI and in the blood early after ATI, prior to viral rebound,were associated with the subsequent achievement of the PTC status. Furthermore, our data suggest that the limitation of replication-competent viral reservoirs during treatment in PLN was related, at least in part, to antiviral CD8+ T responses. These results represent a significant advancement in our understanding of PTC and for clinical HIV remission trials.

Results

PTCs maintain low total SIV-DNA and unspliced cell-associated RNA (caRNA) levels post-ATI in blood and lymph nodes, unlike NCs

We first quantified SIV-DNA and unspliced caRNA longitudinally in total mononuclear cells or isolated $CD4^+$ T cells from blood, as well as in total and $CD4^+$ T cells from PLN (axillary and inguinal LN) (Fig.2). SIV-DNA in blood CD4+ T cells and unspliced caRNA in PBMCs were not different between PTCs and NCs before treatment and similarly dropped upon ART initiation (Fig 2a, b). Differences in SIV-DNA and unspliced caRNA levels between PTCs and NCs were observed after ATI. At day 7 post-ATI, the proportion of animals with detectable total SIV-DNA was significantly higher among NCs (11/11) than among PTCs (7/11) (p=0.027). Significant differences in SIV-DNA levels between PTCs and NCs emerged as early as day 14 post-ATI in circulating $CD4^+$ T cells (median 13 vs 21 copies/10^6 CD4+ T cells respectively; p=0.010; Fig. 2a). A similar dynamic was observed for unspliced caRNA in PBMCs, with lower levels in PTCs compared to NCs from day 28 post-ATI (p=0.006; Fig. 2b). Differences between PTCs and NCs in total SIV-DNA in PBMCs appeared slightly later, reaching significance by day 56 (median 13 vs 21 copies/10^6 PBMCs respectively; p=0.001; Fig. 2c). In NCs, both biomarkers sharply increased after ATI, reaching levels tending toward those observed before ART initiation without changes between D27 post-infection (prior to ART initiation) and more than 6 months after ATI for total SIV-DNA in $CD4^+$ T cells (p=0.492, n=10), unspliced caRNA (p=0.188, n=5),and total SIV DNA in PBMCs (p=0.063, n=5), (Fig. S1a). Inversely, levels remained low without significant evolution in PTCs with no difference between pre-ATI (100 weeks after treatment initiation) and more than 6 months after ATI for total SIV-DNA in $CD4^+$ T cells (p=0.250, n=9,), unspliced caRNA (p>0.999, n=11) and total SIV-DNA in PBMCs (p=0.125, n=11) (Fig. S1b).

In PLN, although no difference was observed between PTCs and NCs before and shortly after ATI in total SIV-DNA (p=0.189 and p=0.146 in PLN CD4+ T cells, Fig 2.d; p=0.595 and p=0.082 in total PLN cells, Fig 2.e) and in unspliced caRNA (p = 0.289 and p=0.502 in total PLN cells, Fig 2.f), levels of SIV-DNA and unspliced caRNA were significantly lower in PTCs compared to NCs more than 6 months after ATI (p<0.001, Figs 2d-f). In NCs, total SIV-DNA levels increased during the 6 months following ATI, both in PLN $CD4^+$ T cells (p=0.031, n=6,) and in total PLN cells (p=0.002, n=10), along with a similar increase in unspliced caRNA levels in whole PLN (p=0.002, n=10), (Fig. S1c). Conversely, levels remained stable in PTCs after ATI, with no significant difference observed between pre-ATI (100 weeks after treatment initiation) and more than 6 months after ATI for total SIV-DNA in PLN $CD4^+$ T cells (p=0.250, n =7) and in total PLN cells (p=0.625, n=9), as well as for unspliced caRNA in whole PLN (p=0.078, n=7), Fig. S1d. Similar kinetics were observed for the unspliced caRNA/SIV-DNA ratios in PBMCs and total PLN cells (Fig. S2a,b). Altogether, while no difference was observed prior to ATI, following ATI, SIV-DNA and unspliced caRNA loads, in blood and PLN, increased markedly in NCs, reaching values significantly higher than those observed in PTCs, for whom no significant change was detected compared to pre-ATI levels.

SIV-DNA levels remain controlled in tissues of PTCs for over 6 months after ATI.

We subsequently quantified SIV-DNA in multiple tissues collected at euthanasia from PTCs, NCs (at least 6 months after ATI) and compared them to levels in never-treated macaques and macaques still on ART at necropsy described in Fig.1 and supplementary table S1. SIV-DNA levels were lower in PTCs compared to NCs and untreated macaques in PBMCs, thymus, secondary lymphoid tissues (spleen, tonsil, peripheral LNs [submandibular, subclavicular, cervical, axillary, iliac, inguinal, popliteal] and deep LNs [recto paracolic and mesenteric]) and multiple sites in gut from stomach to rectum (Fig. 3). Of note, SIV-DNA levels were not significantly different between

PTCs and macaques still under treatment for 2 years. Inversely, reservoir size in NCs did not differ from the macaques that never received ART. Reservoir size did not differ between PTCs and NCs in other non-lymphoid tissues except for skin, bladder, vas deferens, and epididymus body (Fig. S3). Although SIV-DNA levels in the central nervous system were below the quantification threshold, this biomarker was nonetheless more frequently detected in NCs than in PTCs within the frontal, parietal, and occipital lobes (Fig. S4). Finally, when considering all PTCs and NCs macaques together, SIV-DNA in many tissues positively correlated with SIV-DNA in blood compartment and with magnitude of post-ATI plasma viral load (Fig. S5a). Collectively, these findings indicate that blood and tissue reservoir sizes in PTCs remain significantly controlled for an extended period following treatment withdrawal.

SIV transcriptional activity remains controlled in tissues of PTCs for over 6 months after ATI

We then quantified unspliced ca-RNA in multiple tissues at the end of the study. The unspliced caRNA levels in PTCs were comparable to those found in macaques on ART but significantly lower compared to levels in NCs and untreated macaques in PBMCs, thymus, bone marrow, secondary lymphoid tissues (spleen, tonsil, peripheral LNs [subclavicular, cervical, inguinal, popliteal] and deep LNs [recto paracolic and mesenteric]) and every segment of gut from stomach to rectum (Fig. 4). Similar observations were made in various non-lymphoid tissues (liver, pancreas, kidney, lungs, skin, heart, bladder, abdominal and axillary sub-cutaneous adipose tissues, testicles, head and tail epididymus and urethra (Fig. S6). Levels of unspliced caRNA in NCs did not differ from the untreated group, indicating a rapid return upon ATI in these animals to the viral transcriptional activity typically observed during the natural history of SIV infection. When analyzing the unspliced caRNA-to-SIV DNA ratio, similar patterns remained significant across multiple tissues, indicating that in these compartments, SIV DNA was not only quantitatively

restricted but also exhibited reduced transcriptional activity in PTCs compared with NCs (Fig. S2c). Moreover, across all macaques, unspliced caRNA levels in tissues correlated with those in the blood compartment and with the magnitude of post-ATI plasma viral load (Fig. S5b). Together these results indicate a durable control of SIV transcriptional activity in PTCs after ATI in blood, lymphoid tissues and in anatomical sites beyond lymphoid tissues.

Levels of the intact proviruses remain controlled in blood and tissues for over 6 months after ATI in PTCs

Next, the intact proviruses level was estimated in tissues at the end of the study by intact proviral DNA assay (IPDA). The level of intact proviruses was lower among PTCs compared to NCs in multiple tissue types including blood, lymphoid tissues (thymus, spleen, mesenteric and cervical LNs, gut (colon)), and non-lymphoid tissues (lung, liver, adipose tissue) (Fig. 5). Six months after ATI, the intact proviral pool in PTCs was similar to that observed in macaques maintained on continuous ART, whereas NCs exhibited a pool comparable to that of never-treated macaques. When analyzing the unspliced caRNA-to-SIV intact DNA ratio, similar patterns remained significant across multiple tissues, indicating that in these compartments, SIV intact DNA was not only quantitatively restricted but also exhibited reduced transcriptional activity in PTCs compared with NCs (Fig. S2b). Moreover, across all macaques, intact SIV DNA levels in tissues correlated with those in the blood compartment and with the magnitude of post-ATI plasma viral load (Fig. S5c).

The difference between PTCs and NCs at the end of study can logically be attributed to reservoir replenishment by the rebounding virus in NCs. However, as intact proviruses pool is the essential contributor to the rebounding virus, it was worth considering whether this difference preexisted before viral rebound, which could partly explain the subsequent virological rebound or control.

Pre-ATI intact proviruses in lymph nodes predict rebound and reflect CD8$^+$ T cells-mediated control under ART

We quantified intact proviruses within total PLN cells just before ATI (100 weeks after treatment initiation). PTCs exhibited significantly fewer intact proviruses in PLN compared to NCs even before ATI (Fig. 6a). The level of intact proviruses in PLN before ATI was positively correlated with the cumulative viremia after ATI (r=0.688, p=0.003, Fig. 6b) and the viremia assessed at the end of the study (r=0.647, p=0.006, Fig. 6c), predicting the post-ATI replication. Differences between PTCs and NCs in the levels of intact proviruses in PLNs before ATI did not appear to be related, at least not solely, to the delay to ART initiation (Fig. S7a). This was supported by the absence of differences in intact reservoir size in cervical, and mesenteric lymph nodes and PBMCs at euthanasia between early and late-treated macaques without ATI (Fig S7b-d). We therefore wondered if they could be the result of differences in immunological pressure in these animals. In the princeps pVISCONTI report, we showed that PTCs developed stronger SIV-suppressive CD8+ T cell activity[19], including in PLN under treatment (Fig. 6d). We analyzed whether this activity might be associated with intact reservoir in PLNs before ATI. Overall, the SIV-suppressive activity of CD8+ T cells in PLN under treatment was negatively correlated with the level of intact proviruses in these PLNs (spearman correlation, r=-0.590, p=0.047, Fig. 6e). These data suggest that, under treatment, CD8+ T cells might keep driving the selective elimination of cells harboring intact proviruses in PLNs potentially competent for rebound. They also highlight the interplay between immune response and viral reservoir dynamics as key determinants in predicting PTC status. Given the limited accessibility of lymph node tissues, we next explored whether the blood compartment could serve as a surrogate to monitor the intact proviral reservoir and predict rebound.

Levels of intact proviruses measured in blood shortly after ATI predict rebound and mirror intact proviral levels in lymph nodes under ART

To identify more accessible surrogate biomarkers, we analyzed longitudinal (just before ATI, 7 days post-ATI) levels of intact provirus within PBMCs and in blood CD4+ T cells 7 days post-ATI in PTCs and NCs. No difference between PTCs and NCs was observed while on ART, but the pool of intact proviruses in PBMCs significantly increased in NCs upon ATI and remained limited and stable in PTCs until euthanasia (Fig. 7a). Differences in the levels of intact proviruses between PTCs and NCs were observed as early as 7 days post-ATI, both in PBMCs (p=0.048, Fig. 7a) and in isolated CD4+ T cells (p=0.019, Fig. 7b) , preceding the detection of viral rebound in plasma (at 7 days post-ATI, median plasma viral loads: 2 vs. 1 cp/mL for PTCs (n=11) and NCs (n=11) respectively; p=0.900, Fig. 7c). These differences were not observed when macaques were compared based on treatment initiation timing (Fig. S7e-f). Overall, intact SIV DNA levels in PBMCs and circulating CD4+ T cells 7 days post-ATI were correlated with both cumulative viremia post-ATI (r=0.488, p=0.021 for PBMCs, Fig. 7d, r=0.608, p=0.004 for CD4+T cells, Fig. 7e;) and viremia at the end of the study (r=0.499, p=0.018 in PBMCs Fig. 7f and r=0.535, p=0.012 in CD4+T cells, Fig. 7g). While the level of intact proviruses in PLN prior to ATI did not correlate with that in PBMCs at day 7 post-ATI (r = 0.500, p = 0.040; Fig. 7h), it correlated with that in circulating $CD4^+$ T cells (r = 0.500, p = 0.040; Fig. 7i), suggesting that $CD4^+$ T cells after ATI but before viral rebound may retrospectively reflect the intactness of the PLN reservoir prior to ATI.

These findings support the use of intact provirus quantification in blood-derived $CD4^+$ T cells after ATI and before rebound, as a surrogate biomarker of the intact reservoir in PLN under treatment, and as an early predictor of viral rebound.

Immune features associated with reservoir virological parameters measured at the end of the study

We next examined whether previously determined parameters of the humoral and the $CD8^+$ T cell response[19] correlated with the size, transcriptional activity, and intactness of the reservoir at euthanasia. Univariate spearman analyses revealed that anti-gp140 IgG responses after ATI, correlated positively with reservoir parameters (total SIV DNA, unspliced caRNA, and intact proviruses), likely reflecting the indirect effect of stronger viral rebound driving both enhanced antibody responses and reservoir reseeding. This observation is consistent with findings in PLWH, where antibody levels mirrored total HIV DNA load in PBMCs rather than predicting virological control after ATI[43]. In contrast, greater pre-ATI $CD8^+$ T cell suppressive capacity in PLN, as well as a higher post-ATI magnitude of anti-SIV suppressive activity in blood, quantified as the area under the curve (AUC), were associated with a more restricted reservoir across multiple tissues, in terms of size, transcriptional activity, and intactness. Similarly, high SIV-specific $CD8^+$ T cell polyfunctionality, defined by the simultaneous production of IFN-γ, TNF-α, IL-2 and CD107a in blood at euthanasia, was linked to a more restricted reservoir profile, whereas single cytokine production showed no significant associations (Fig. 8a).

Regarding proliferative features, increased intracellular Ki67 expression correlated with reduced reservoir measures in two distinct settings: in total and central memory $CD8^+$ T cells from lymph nodes at day 14 post-ATI, and in central memory $CD8^+$ T cells from blood at day 28 post-ATI. A higher expression of CCR7 (lymphoid recirculation), TCF1 (self-renewal capacity), and lower expression of PD-1 (preserved functional capacity) on SIV-specific memory $CD8^+$ T cells in spleen at euthanasia had previously been described in PTCs compared to NCs in this model [19]. We extended these observations by showing that this profile of long-lived and stem-like memory SIV-

specific $CD8^+$ T cells was associated with a more comprehensively defined restriction of the reservoir, involving its size, transcriptional activity, and intactness across multiple tissues. Conversely, higher reservoir measures were associated with an early accumulation of differentiated effector $CD8^+$ T cells shortly after ATI (day 14 post-ATI), suggesting ineffective responses unable to contain rebound, and with increased $CD8^+$ T cell activation ($CD38^+HLA\text{-}DR^+$) at euthanasia (Fig. 8b). Together, these results suggest that the long lived and stem like properties of memory SIV specific $CD8^+$ T cells, characterized by a central memory phenotype with high proliferative capacity and absence of activation traits, contribute through an enhanced SIV suppressive capacity, to shaping a smaller total and intact reservoirs with reduced transcriptional activity across tissues, emphasizing the potential role of these qualitative immune features in maintaining post treatment control.

Proviral genetic evolution is durably restricted in PTCs

To better understand the dynamics of the proviruses, genetically intact proviral sequences were isolated at the end of the study from PBMCs and various tissues, including non-lymphoid organs known to contribute to reservoir persistence (e.g., lungs[44–46] and kidneys[47–49]), in five PTCs (three early-treated and two late-treated macaques) and five NCs (two early-treated and three late-treated macaques), as summarized in Supplementary Table S1. For non-lymphoid tissues (kidneys and/or lungs), because of the very low reservoir levels, NFL amplification could not be achieved for all macaques, which accounts for the limited data available for 6 out 10 animals. In parallel, the complete genome of the SIVmac251 inoculum used for infection, as well as viral genomes from circulating viruses at multiple time points (primary infection, treatment initiation at week 4 or week 24 post-infection, viral rebound, and euthanasia in NCs), were sequenced. Pairwise

genetic distances were calculated to quantify viral divergence among the inoculum, circulating viruses at these time points, and intact proviruses derived from tissues and blood for each macaque. This analysis revealed two distinct evolutionary profiles based on PTC status (Fig 9, Fig. 10, Fig. S8). Although no significant difference was observed in the genetic distance between the inoculum and plasma SIV RNA genomes prior to treatment between PTCs and NCs, intact proviruses from various tissues at the end of the study were genetically closer to the inoculum in PTCs compared to NCs (Fig. 9a). This difference reached statistical significance in LNs (cervical and mesenteric) and gut tissues (colon and ileum), while PBMCs showed a trend approaching significance (p= 0.057). Additionally, intact proviruses in PTCs at the end of the study were genetically closer to plasma SIV RNA genomes sampled during primary infection compared to NCs (Fig 9b), with significant differences observed in LNs (cervical and mesenteric). No such difference was observed when comparisons were made according to the timing of ART initiation (Fig s8a-b). Limited proviral evolution in PTCs was further supported by phylogenetic analyses showing that proviruses remained genetically close to the original infectious strain (Fig 10a). In contrast, although a few ancestral variants were present at the end of the study, most intact proviruses in NCs formed distinct and large clusters separated from the inoculum and pre-ART circulating virus genomes, defined as monophyletic groups supported by ≥90% bootstrap (Fig. 10b). Intact proviruses in tissues of NCs clustered closely together regardless of their anatomical location (Fig. 10b, Fig. S8). They were significantly genetically closer to viral genomes circulating at the time of rebound and treatment initiation than to those from primary infection, which were significantly more genetically distant (Fig. S8 and S10Fig. S10a-d: significant for PBMCs, ileum and LN [cervical and mesenteric]). Additionally, viral genomes circulating at rebound were significantly genetically closer to those present at the time of treatment initiation than to those

from earlier time points, particularly primary infection (Fig. S8 and S10e). Overall, these findings demonstrate that, unlike NCs, PTCs exhibit a durable restriction in proviral evolution, consistent with a strong control of reservoir extension in the PTCs following ATI.

Discussion

The PTC status in this NHP model was associated with a controlled reservoir in terms of size, transcriptional activity, proviral evolution and intactness in the blood and various tissues, even long after ATI. At euthanasia, total SIV-DNA, caRNA, and intact provirus levels in PTCs were comparable to those observed in macaques continuously maintained on ART for two years, highlighting sustained and effective control of viral replication and the SIV reservoir. In contrast, in NCs, these biomarkers rapidly returned to levels typically observed during the natural course of SIV infection in untreated macaques due to reservoir replenishment following viral rebound. While such control has been observed in human PTCs within the blood compartment[15,25,50] and rectal tissue[27] our study demonstrates that SIV reservoir control after ART interruption in this model is spread throughout multiple anatomical sites.

Tissue proviruses in PTCs, long after ATI, remained genetically closer to the original inoculum and to viral genomes circulating at the time of primary infection compared to NCs, which harbored genetically well-differentiated proviruses. This difference is likely due to the proviral evolution triggered by the reignited viral replication and reservoir replenishment following ATI in NCs. In these macaques, viral genomes circulating at rebound were significantly genetically closer to those present at the time of treatment initiation than to those from earlier time points. This result is consistent with a previous study in PLWH showing that viral rebound primarily originated from circulating viruses immediately prior to the ART initiation[51]. This result is typically consistent with the “last-in first-out” hypothesis, a theoretical concept suggesting that viruses replicating just before ART initiation, lastly integrated (last-in) are most likely to drive viral rebound when ART is stopped (first out)[52]. This hypothesis suggests that the circulating virus present at the time

of ART initiation is better adapted to the host immune environment than previously circulating variants and is therefore more likely to re-emerge after treatment interruption.

Of note, our study revealed several reservoir characteristics that distinguished PTCs and NCs pre-ATI. Notably, PTC was preceded by lower levels of intact proviruses, those more likely to be competent for viral rebound,in PLN prior to ATI (100 weeks after ART initiation). LNs and the gut have both been recognized as major sites of reservoir persistence under ART and potential contributors to viral rebound, although their respective contributions remain debated[36,53,54]. Our findings further suggest that PLNs may play a particularly important role in driving viral rebound. In PLN before ATI, the pool of intact proviruses correlated with the post-ATI viremia (cumulative and at the end of the study). Importantly, this pool was also negatively correlated with the SIV-suppressive activity of CD8+ T cells in PLN. These results point to a central role of the immune response in shaping the viral reservoir in PLN while on ART by eliminating infected cells harboring intact proviruses.Therefore, a reduced pool of potentially replication-competent proviruses under ART in PLN may depend on the effectiveness of adaptive effector cell responses honed upon ART initiation. It is tempting to assume that a context where the pool of intact proviruses is reduced by enhanced immune-mediated elimination, provides an optimal opportunity for virological control after therapy interruption. Additionnaly, long-lived and stem like properties of memory SIV specific $CD8^+$ T cells, were associated with smaller total and intact reservoirs with reduced transcriptional activity across tissues long after ATI, emphasizing their potential role in maintaining post treatment control[19]. Our observations reinforce a central role of $CD8^+$ T cells in PTCs[19], echoing earlier findings on the natural control of SIV[55] and highlight them as key targets for immunotherapy strategies aimed at achieving HIV remission. Those observations do not exclude potential additional immune mechanisms that may contribute to PTC. Innate immune

responses, including NK cells [25,56–58], could participate in this clearance by modulating $CD8^+$ T cell function or exerting direct antiviral effects. Beyond NK and $CD8^+$ T cells, other immune pathways may also participate in limiting viral rebound, including type I interferon-driven intrinsic restriction pathways, CARD8-mediated inflammasome activation, and antibody-dependent effector functions. As recently reviewed by Armani-tourret *et al.*[59], these complementary mechanisms likely act in concert with adaptive immunity to shape the rebound-competent reservoir. To complement the control of intact provirus levels, it is also possible that immune pressure selectively favors the persistence of intact proviruses integrated into transcriptionally silent chromatin which may be less prone to reactivation after ATI[52,60]. Our observations, showing that in most tissues both total and intact proviruses were not only quantitatively restricted but also exhibited reduced transcriptional activity in PTCs, are consistent with this hypothesis and support the existence of a "block-and-lock" state of the reservoir. Further investigations are required to define how these immune and epigenetic mechanisms may interact to shape the rebound-competent reservoir.

To date, several predictive biomarkers of PTC have been proposed, but none is sufficient so far for clinical use[61–63]. Identifying factors that predict maintained virological control after ATI is crucial for designing and evaluating interventions aimed at achieving HIV remission. In PLWH treated during the chronic stage, but not in those treated during the early stage, the size of the intact provirus pool in blood prior to ATI has been shown to correlate with the time to HIV rebound after treatment interruption, although it does not predict prolonged post-treatment control[61]. Similarly, when analyzing the entire CHAMP cohort, no difference in the intact provirus pool in blood, as assessed by IPDA, was observed prior to ATI based on subsequent off-therapy control[25]. Here, a high SIV-suppressive activity of CD8+ T cells, combined with a smaller intact

proviral reservoir in PLN, defines a robust immunovirological profile associated with sustained viral control. While lymph nodes are central to understanding PTC, PLN biopsy remains an invasive procedure that is rarely performed, even in clinical studies or trials. Hence, the development of blood predictors is warranted. Although we observed no significant difference in intact proviral levels in PBMCs prior to ATI, likely due to the lower frequency of infected cells in blood, such differences emerged as early as day 7 after ATI, before detectable plasma rebound, in both PBMCs and $CD4^+$ T cells. These findings suggest that blood-based quantification of intact proviruses shortly after ATI reflects the amount of intact proviruses in PLN under treatment, and could serve as an early and non-invasive predictor not only of rebound timing, but also of sustained post-treatment control.

Our study has some limitations, particularly the sample size, which, while adequate for identifying meaningful results and adhering to ethical principles of animal model research, restricted the feasibility of certain statistical analyses. Although the amount of tissue collected was substantial for most analyses, some samples were not available at specific times, in order to respect ethical considerations. In addition, relying solely on unspliced cell-associated RNA provides an incomplete picture of residual transcriptional activity, as different RNA species (total, elongated, polyadenylated, and multiply spliced transcripts) reflect distinct stages of transcriptional progression and blockade. A more granular characterization of SIV transcription would therefore represent a valuable approach to further elucidate the mechanisms underlying reservoir persistence and post-treatment control[64]. However, the available material constrained the number of biomarkers that could be consistently measured across all animals and tissues.

In summary, we have formally demonstrated in a NHP model the prolonged control of blood and deep tissue reservoirs in PTCs. Our data suggest that the development of enhanced SIV-

suppressive activity of CD8+ T cells upon ART initiation in PTCs drives a decrease in the pool of intact proviruses in PLN, which contributes to the successful prolonged off-therapy virological control. Although the less invasive biomarker identified requires sampling shortly after ART interruption, it could still be explored as a potential criterion for selecting PLWH for ATI in HIV cure research, given the minimal risk of reservoir replenishment, transmission, or resistance selection before viral rebound. In conclusion, this study enhances our understanding of the factors that are critical for PTC and contribute to the identification of biomarkers for clinical HIV remission trials.

Methods

Ethical statement[19]

CyMs were imported from Mauritius and housed in facilities at the Infectious Disease Models and Innovative Therapies (IDMIT) center (CEA site in Fontenay-aux-Roses, France). All nonhuman primate studies at IDMIT were conducted in accordance with French national regulations (CEA Permit Number D92-032-02). IDMIT complies with the standards for Human Care and Use of Laboratory Animals of the Office for Laboratory Animal Welfare under Assurance Numbers #A5826-01 and #F20-00448. All experimental procedures were conducted according to European Directive 2010/63 (Recommendation Number 9). The pVISCONTI study was approved and accredited under the statement A15 035 from the "Comité d'Ethique en Expérimentation Animale du CEA" and was registered and authorized under Number 2453-2015102713323361v3 by the French Ministry of Education and Research. Experimental procedures (animal handling, viral inoculations, and samplings) were conducted after sedation with ketamine chlorhydrate (Imalgene 1000®, 10 mg/kg, intravenously (i.v.), Merial). Tissues were collected during follow-up and at necropsy. Animals were euthanized after ketamine chlorhydrate sedation followed by a bolus of sodium pentobarbital (Doléthal, 180 mg/kg, i.v., Laboratoire Vetoquinol).

Study design[19]

SIVmac251-infected CyMs were classified as PTCs (n=11, 9/11 treated at W4 pi, 2/11 treated at W24 pi) when they were able to decrease their plasma viremia below 400 copies/ml following the initial viral rebound or if they never experienced viral rebound. Animals that did not meet these criteria were classified as NCs (n=11, 2/11 treated at W4 pi, 9/11 treated at W24 pi)(Fig. 1).[19]. PTCs and NCs were monitored for at least 6 months after ATI before euthanasia. Sixteen untreated macaques and 11 virologically suppressed treated macaques without ATI (ART

initiation at W4 (n=5) and at W24 (n=6)), were used as controls. In treated animals without ATI, euthanasia occurred following 2-year treatment. In untreated macaques, euthanasia occurred more than 6 months after infection.The study design and the viral loads of the CyM groups (never-treated macaques, NCs, PTCs and treated macaques without ATI) are shown in Fig. 1. The characteristics of the CyMs included in this study and exact euthanasia time points are provided in Supplementary Table S1. The samples used for virological analyses are described in Fig. S11 and in the Source date file, where each sheet provides the values underlying a given figure or figure panel, along with the identities of the corresponding CyMs.

Animals and experimental condition, blood and tissue collection and processing

Animals and experimental conditions, blood and tissues collection and processing, have been throughly described in Passaes *et al.*[19]. Antemortem PLN, including axillary and inguinal nodes, were collected immediately prior to ATI—100 weeks after ART initiation and 14 days after ATI. At necropsy, tissues samples were collected and directly stored at minus 80 C° as dried, pretreated with RNA later (Invitrogen AM7020) or RPMI conditioned biopsies. It included thymus, bone marrow, spleen, tonsil, LNs (mesenteric, iliac, recto paracolic, axillary, inguinal, popliteal, cervical, subclavicular, submandibular), gut segments (stomach, duodenum, jejunum, caecum, terminal ileum, ascending colon, transversal colon, descending colon, sigmoid, rectum), liver, pancreas, kidney, lungs, skin (site injection and other sites), heart, central nervous system (frontal, occipital, parietal lobes, cerebellum, brainstem), adipose tissues (visceral, subcutaneous abdominal, subcutaneous axillary, brown), bladder, epididymus (head, body, tail), seminal vesicle, prostate, vas deferens and urethra. LN cells were isolated into RPMI medium via mechanical disruption using gentel-MACS dissociator (Miltenyi Biotec). The cell suspension was filtered (70µm) and red blood cells were lysed in ACK. When applicable, $CD4^+$ T cells were isolated

using nonhuman primate CD4+ Microbeads with MultiMACS TM Cell24 Separator (Miltenyi Biotec).

Quantification of plasma viral load

As previously described[19], plasma viremia was monitored longitudinally in all animals using quantitative RT-PCR targeting *gag* region, performed using a SuperScript III Platinum One-Step qRT-PCR kit (Thermo Fisher Scientific) with a CFX96 Touch Real-Time PCR Detection System (Bio-Rad). Limit of detection was 12.3 copies/mL.

SIV-DNA and cell-associated unspliced SIV-RNA (caRNA)

As described previously[19], DNA and RNA were extracted from PBMCs with an AllPrep DNA/RNA Mini Kit (Qiagen). DNA from $CD4^+$ T cells isolated from blood and lymph nodes was extracted using the QIAamp DNA Micro Kit, optimized for low cell input. For tissue, to control for differences in viral distribution within a single organ, two or three tissue samples were mechanically disrupted separately with a MagNA Lyser (GmbH, Roche Diagnostics, Brussels, Belgium). Each tissue sample was first mechanically disrupted, and the resulting lysate was divided into two aliquots: one for DNA extraction (DNA Mini Kit, Qiagen) and the other for RNA extraction (RNeasy Plus Mini Kit, Qiagen). RNA extraction included a DNase I treatment (Qiagen).

Total SIV-DNA was quantified by ultrasensitive real-time PCR targeting the *gag* region[65]. SIV-DNA levels were expressed as copies per 10^6 cells, based on quantification of the cellular CCR5 gene by qPCR. The CCR5 assay used an equimolar mix of two forward primers (5'-CAACATGCTGGTCGATCCTCAT-3' and 5'-CAACATACTGGTCGTCCTCATCC-3'), a reverse primer (5'-CAGCATAGTGAGCCCAGAAG-3'), and a probe (5'-HEX-CTGACATCTACCTGCTCAACCTG-BHQ1-3'). The total SIV-DNA limit of quantification (LoQ) was 13 copies per 10^6 cells. SIV caRNA was quantified by one-step real-time RT-PCR targeting the *gag* region[65]. Normalization of SIV caRNA

was performed with ribosomal RNA (one-step real-time PCR using the Ribosomal RNA Control Reagents Kit (Applied Biosystems)).The caRNA LoQs were 10 and 30 copies/μg of total RNA in tissues and cells respectively.

Estimation of intact SIV proviruses levels

SIV proviruses intactness was estimated longitudinally in PBMCs and PLN as well as in PBMCs and multiple tissues (thymus, spleen, mesenteric LN, cervical LN, ileum, ascending colon, rectum, liver, kidney, lungs, subcutaneous axillary adipose tissue) at the end of the study. Levels of intact SIV proviruses were estimated by the Intact Provirus DNA Assay (IPDA) previously described to address the critical need for a scalable method to estimate the intact HIV-1 reservoir[66]. The method was adapted to the SIV by Bender *et al*[67]. Briefly, assay is based on a multiplex ddPCR amplifying simultaneously two SIV regions (*pol* and *env*) to distinguish potentially intact proviruses (positive probe signals from both regions) from a large number of defective proviruses. DNA shearing and cell equivalents is assessed by another ddPCR based on 2 probes in CyMs RPP30 gene spaced at the same distance as that separating the SIV targeted regions. Finally, 2LTR SIV-DNA episomal forms are assessed by a third ddPCR to subtract them from the intact proviruses[68]. Oligonucleotide sequences of primers and probes used for IPDA are provided as separate Supplementary Data 1. IPDA was performed on the QX200 ddPCR system (Biorad). Before ddPCR, extraction adapted for tissues (DNeasy Blood & Tissue kit, Qiagen) was performed to limit DNA shearing to preserve DNA integrity and ensure an accurate measurement of intact proviruses. The DNA shearing index (DSI) was used to correct IPDA results, as previously described[69]. Only extracts with a DSI equal or under 0.5, confirming the preservation of DNA integrity, were retained for analysis. RPP30 ddPCR was performed from 8 ng of genomic DNA.

For SIV proviruses ddPCR quantification, samples were deposited in replicates (from 2 to 8) to reach a minimum of 700 ng DNA per sample corresponding to 100,000 cells. Results from replicates were merged and analyzed using the QX Manager Software 2.1.0.25 Standard Edition. The absolute intact proviruses amount was corrected by DSI and reported per 10^6 cells quantified by the RPP30 ddPCR.

Near-full-length SIV genome sequencing

Near-full-length (NFL) SIV genome sequencing was conducted with the nanopore technology in samples from 5 PTCs (3 treated at W4 pi, 2 treated at W24 pi) and 5 NCs (2 treated at W4 pi, 3 treated at W24 pi). This composition was chosen to mitigate the potential bias due to differences in the timing of treatment initiation. SIV proviruses were sequenced from PBMCs and various tissues at the end of the study, including thymus, spleen, cervical and mesenteric LN, ileum, colon, rectum, lungs, kidney, depending on their availability in sufficient quantities. If plasma was available, circulating SIV RNA was sequenced at primary infection, W4 pi and at W24 pi (for macaques treated at W24 pi). For NCs, plasma SIV RNA was also sequenced at the time of viral rebound and at the end of the study. The inoculum that served for initial infection was sequenced to track genetic evolution. Dilution conditions were determined separately for each sample and used for the first PCR. Near-full-length SIV DNA was amplified from the 5'-LTR to the 3'-LTR with a nested PCR using PrimeSTAR GXL DNA polymerase (TaKaRa) with, for the outer PCR, forward primer 5'-CTCCACGCTTGCTTGCTTA-3' and reverse primer 5'- CCTGCTAGTGCTGGAGAGAACC-3' at a final concentration of 0.3 μM in 30 μL. From 5 μL of the first PCR mixture, the inner PCR was performed using the forward primer 5'- GTGTGTGTTCCCATCTCTCCTA-3' and the reverse primer 5'-AACCTCCCAGGGCTCAATCT-3' at a final concentration of 0.2 μM in 50 μL. PCRs were carried out using the following program: 98°C for 2 min, followed by 98°C for 10 s, 54°C or 60°C (for the

outer and inner PCR, respectively) for 15 s, and 68°C for 9 min 30 for 40 cycles, and then 10°C indefinitely. Positive nested PCR products were identified by electrophoresis on a 1% agarose gel and purified with column (QIAquick PCR purification Kit). Plasma SIV RNA was reverse-transcribed before amplification using the SuperScript IV (Invitrogen by Life Technology) with the reverse primer of the outer PCR described above at a concentration of 0.1 μM in a final volume of 20 μL. Library preparations were performed from 400 ng of purified PCR products using the SQK-LSK109 kit following the native barcoding genomic DNA protocol from ONT (NBE_9065_v109_revAP_19Jan2021). Samples were multiplexed by using the native barcode kit EXP-NBD196. To enrich long fragments, purification after adapter ligation was performed based on SPRI size selection protocol for >1.5-2 kb DNA fragment (v1, 22.01.28) adapted from the work of M. Schalamun and B. Schwessinger (https://www.protocols.io/view/dna-sizeselection-1kb-and-clean-up-using-an-optimidmca46). A total amount of 150-300 ng of the final library, corresponding of 23-46 fmol of 10 kB fragments was sequenced on FLO-MIN106 flow cells (R9.4.1). Single molecule near full-length SIV genome nanopore sequencing was run until exhaustion of nanopores (72h) on a GridION platform. Basecalling and demultiplexing was performed by MinKNOW v23.07.12 based on guppy v7.1.4.

Haplotype reconstruction and sequence analyses

To reconstruct viral haplotypes, we applied RVHaplo clustering algorithm to group into the same cluster reads originating from the same haplotype[70]. This reference-guided pipeline cluster reads according to their similarity into several haplotypes. After alignment against SIVmac251 reference (accession number: KU892415), haplotypes were retained if present with a minimum frequency of at least 5% and supported by at least 100 high quality reads of at least 9,000 nucleotides. Proviruses with deletions (>100 bp) were considered defective[7,71]. Deleterious stop

codons were identified using the Gene Cutter tool (Los Alamos HIV Database; https://www.hiv.lanl.gov/content/sequence/GENE_CUTTER/cutter.html). Any contigs containing a stop codon were considered defective. APOBEC-induced (apolipoprotein B mRNA-editing enzyme, catalytic polypeptide-like–induced) G–A hypermutations were identified using the Los Alamos HIV Database Hypermut 2 program (https://www.hiv.lanl.gov/content/sequence/HYPERMUT/hypermut.html). Defective proviruses characterized by hypermutations, large deletions, defaults ψ encapsidation signal were not included in the downstream analyses. Viral divergence was quantified by calculating the mean pairwise genetic distance between proviral haplotypes from tissues sampled across anatomical sites and SIV RNA NFL genomes from circulating viruses at various study time points, using the Tamura-Nei (TN93) correction for multiple hits[72,73]. A maximum likelihood (ML) phylogeny including all haplotypes from each animal was estimated using IQ-TREE with the general time-reversible (GTR) substitution model[74].

Measurement of SIV suppressive activity

Autologous CD4+ and CD8+ T cells were purified from freshly isolated PBMCs or tissue cell suspensions by positive and negative selection, respectively, using non-human primate CD4+ MicroBeads and CD8+ T Cell Isolation Kit, with the MultiMACS™ Cell24 Separator (Miltenyi Biotec). Purified CD4+ T cells were stimulated for 3 days with concanavalin A (5µg/mL, Sigma-Aldrich) in the presence of IL-2 (100 IU/mL, Miltenyi Biotec). Purified CD8+ T cells were cultured in the absence of mitogens and cytokines (ex vivo CD8+ T cells). Stimulated CD4+ T cells (105) were superinfected in U-bottom 96-well plates with a standardized SIVmac251 inoculum (MOI = 10^{-3}), ensuring identical levels of infection across macaques at baseline an thereby overcoming the contribution of endogenous virus replication, . Superinfection was performed either in the

presence (1:1 effector-to-target-cell ratio) or absence of ex vivo CD8+ T cells (105) from the same tissue via spinoculation for 1 hour (1,200g at room temperature) and incubated for 1 hour at 37°C. Cells were then washed and cultured in R10 medium containing IL-2 (100 IU/mL, Miltenyi Biotec). Culture supernatants were assayed on day 7 using an SIV p27 Antigen ELISA Kit (XpressBio). Antiviral activity was calculated as $\log_{10}$ (mean p27 ng/mL in SIV-infected CD4+ T cell cultures without ex vivo CD8+ T cells) / (mean p27 ng/mL in SIV-infected CD4+ T-cell cultures with ex vivo CD8+ T cells)[55,75].

Analyses of T-cell activation and proliferation markers

As previously detailed[19], total T-cell activation and proliferation were assessed using fresh PBMCs and tissue cell suspensions. Cells were stained with the LIVE/DEAD Fix- able Aqua Dead Cell Stain Kit (Thermo Fisher Scientific) and then surface stained for CD3, CD4, CD8, CD38, and HLA-DR. For differentiation phenotype analyses, cells were additionally stained with CD45RA, CCR7 and CD27. Then, the cells were fixed/permeabilized using a Cytofix/ CytoPerm Kit (BD Biosciences) and stained for intracellular Ki-67. The following antibodies were used: anti-CD3–AF700 (clone SP34-2, BD Biosciences), anti-CD4–PerCP-Cy5.5 (clone L200, BD Biosciences), anti- CD8–APC-Cy7 (clone RPA-T8, BD Biosciences), anti-CD38–FITC (clone AT-1, StemCell Technologies), anti-HLA-DR–V450 (clone G46-6, BD Biosciences), anti-CD45RA–PE Cy7 (clone 5H9, BD Biosciences), anti- CCR7–PE-Dazzle594 (clone G043H7, Biolegend), anti-CD27–PE (clone M- T271, BD Biosciences), and anti-Ki-67– AF647 (clone B56, BD Bios- ciences). Data were acquired using an LSRII flow cytometer (BD Bios- ciences) and analyzed with FlowJo software version 10 (Tree Star Inc.). Cells were classified as follows: naive—CD45RA+CD27+CCR7+; central memory (CM)—CD45RA−CD27+CCR7+;

transitional memory (TM)— CD45RA-CD27+CCR7-; effector memory (EM)— CD45RA−CD27−CCR7−; and effector—CD45RA+CD27-CCR7−.

Cytokine production, memory and proliferative capacity of SIV-specific T cells

As previously detailed[19], frozen PBMCs were thawed, resuspended at 1×10^6/mL in R20 medium, and incubated overnight at 37 °C. Cells were then stimulated with a pool of 24 optimal SIV peptides (8–10 amino acids, 2μg/mL each) in the presence of anti-CD28 (1μg/mL, clone L293, BD Biosciences) and anti-CD49d (1 μg/mL, clone 9F10, BD Biosciences) and stained with anti-CD107a (clone H4A3, BD Biosciences) for 30 min prior to the addition of GolgiStop (1 μL/mL, BD Biosciences) and brefeldin A (BFA, 5 μg/mL, Sigma-Aldrich). Costimulatory antibodies alone were used as a negative control, and concanavalin A (5μg/mL, Sigma-Aldrich) was used as a positive control. Cells were incubated for a total of 6 hr. To evaluate the differentiation profile, cells were stained with the LIVE/DEAD Fixable Aqua Dead Cell Stain Kit (Thermo Fisher Scientific) and then surface stained for CD3, CD4, CD8, CD45RA, CCR7, CD27 and CD127. Cells were then fixed/permeabilized using the Cytofix/CytoPerm Kit (BD Biosciences) and stained intracellularly for IFNγ, TNFα, and IL-2. The results were corrected for background by subtracting the negative (no peptide) control from the peptide- stimulated response. To evaluate the memory profile, cells were stained with the LIVE/DEAD Fixable Aqua Dead Cell Stain Kit (Thermo Fisher Scientific) and then surface stained for CD3, CD8, CD45RA, CCR7, CD27, CD39, and PD-1 in brilliant stain buffer (BD Bioscience). Cells were then fixed/permeabilized using Phosflow buffer (BD Biosciences) and stained intracellularly for TCF-1, IFNγ and TNFα.

CD8+ T-cell proliferation upon stimulation was evaluated by CFSE staining (1 μM, Thermo Fisher Scientific). PBMCs were CFSE stained, stimulated with a pool of 24 optimal SIV peptides (2 μg/mL each), and then cultured for 6 days. Twelve hours before completing the total incubation time, an additional dose of the peptides was added as well as GolgiStop (1 μL/mL, BD Biosciences), brefeldin A (BFA, 5 μg/ mL, Sigma-Aldrich), and an anti-CD107a antibody. Unstimulated cells were used as a negative control. Cells were stained with the LIVE/DEAD Fixable Aqua Dead Cell Stain Kit (Thermo Fisher Scientific) and then surface stained for CD3, CD4, CD8, CD45RA, CCR7, CD27 and CD127. Cells were then fixed/permeabilized with PhosFlow fix/perm buffers (BD Biosciences) and stained intracellularly for IFNγ, TNFα, IL-2, pS6 Ser235/236 and anti-pAKT Ser473.

The following antibodies were used: anti-CD3–AF700 (clone SP34-2, BD Biosciences), anti-CD4–PerCP-Cy5.5 (clone L200, BD Bios- ciences), anti-CD8–APC-Cy7 (clone RPA-T8, BD Biosciences), anti- CD45RA–PE Cy7 (clone 5H9, BD Biosciences), anti-CCR7–PE-Dazzle594 (clone G043H7, Biolegend), anti-CD27–PE (clone M-T271, BD Biosciences), anti-CD127–BUV496 (clone HIL-7R-M21, BD Biosciences), anti-CD107a–BV786 (clone H4A3, BD Biosciences), anti-TNFα–BUV395 (clone MAb11, BD Biosciences), anti-IFNγ–BV605 (clone B27, BD Bios- ciences), anti-IL2–BUV737 (clone MQ1-17H12, BD Biosciences), anti-phospho S6 S235/236–Pacific blue (clone D57.2.2E, Cell Signaling), anti-phospho Akt Ser473–AF647 (clone D9E, Cell Signaling), anti- CD279 (PD1)-BV 421 (clone EH12.2H7, Biolegend), anti-CD39-BV785 (clone A1), and anti-TCF-7/TCF-1-FITC (clone S33-96, BD Bioscience). Data were acquired using a Fortessa flow cytometer (BD Biosciences) and analyzed with FlowJo software version 10 (Tree Star Inc.). The results were corrected for background by subtracting the negative (no peptide) control from the peptide-stimulated response. Negative responses were given an arbitrary value of 0.01.

Titration of SIVmac251 gp140 IgG

SIVmac251 g140-foldon-type glycoproteins were produced by transient transfection of FreeStyle™ 293-F cells and purified by affinity chromatography using Ni Sepharose® Excel beads (GE Healthcare). High- binding 96-well ELISA plates (Costar, Corning) were coated overnight with 250ng/well of purified recombinant SIV gp140 protein. After washing with 0.05% Tween 20-PBS (washing buffer), plates were blocked for 2 h with 2% BSA, 1 mM EDTA, and 0.05% Tween 20-PBS (blocking buffer), washed, and incubated with serially diluted NHP sera in duplicate at 1:250 or 1:50 followed by 7 consecutive 1:4 or 1:3 dilutions in PBS for IgG detection, respectively. After washing, the plates were revealed by incubation for 1 h with goat HRP-conjugated anti-human IgG antibodies (Jackson ImmunoReseach, 0.8 µg/ml final) and by adding 100µl of HRP chromogenic substrate (ABTS solution, Euromedex). Optical densities were measured at 405nm (OD405 nm), and background values based on incubation of PBS alone in coated wells were subtracted. Experiments were performed using a HydroSpeed™ microplate washer and Sunrise™ microplate absor- bance reader (Tecan Männedorf, Switzerland).

Statistical analyses

For statistical analyses, detectable but below the LoQ values for SIV-DNA and caRNA loads were adjusted to threshold values, with undetectable loads defined as half the threshold. Non-parametric tests were employed for the analyses. Group comparisons were made using the Mann-Whitney and Kruskal-Wallis tests. For paired data, the Wilcoxon matched-pairs rank test and Friedman test were used. Proportions between groups were compared using Fisher's exact test. Correlations were assessed using spearman rank analyses. All other statistical analyses were performed using GraphPad Prism version 10.1.1 (GraphPad Software). No adjustments were

made for multiple comparisons, given the exploratory nature of the analyses. All tests were two-sided, and P-values < 0.05 were considered statistically significant. Exact P values and sample sizes are provided in the first sheet of the Source data file.

Data availability

Sequencing data generated in this study (proviral DNA sequences from tissue samples collected at euthanasia and plasma viral RNA sequences from longitudinal timepoints) have been deposited in the Sequence Read Archive (SRA) under BioProject accession code PRJNA1256680 [http://www.ncbi.nlm.nih.gov/bioproject/1256680]. Basecalled FASTQ files are provided for all runs. Metadata for each macaque, tissue type and timepoints are included in the associated BioSamples. Additionnaly, the data that support the findings of this study are presented in the main figures and Supplementary Information/Source Data files. Source data are provided with this paper. Further information and requests for resources and reagents should be directed to the lead contact. Request for biological resources will be fulfilled based on availability and upon the establishment of an MTA.

References

1. Avettand-Fènoël, V. *et al.* Total HIV-1 DNA, a Marker of Viral Reservoir Dynamics with Clinical Implications. *Clin. Microbiol. Rev.* **29**, 859 (2016).
2. Calin, R. Treatment interruption in chronically HIV-infected patients with an ultralow HIV reservoir. *AIDS* **30**, (2016).
3. Li, J. Z. Time to viral rebound after interruption of modern antiretroviral therapies. *Clin Infect Dis* **74**, (2022).
4. Li, J. Z. The size of the expressed HIV reservoir predicts timing of viral rebound after treatment interruption. *AIDS* **30**, (2016).
5. Wong, J. K. Recovery of replication-competent HIV despite prolonged suppression of plasma viremia. *Science* **278**, (1997).
6. Chomont, N. HIV reservoir size and persistence are driven by T cell survival and homeostatic proliferation. *Nat Med* **15**, (2009).
7. Hiener, B. *et al.* Identification of Genetically Intact HIV-1 Proviruses in Specific CD4+ T Cells from Effectively Treated Participants. *Cell Rep.* **21**, 813–822 (2017).
8. Chun, T.-W. *et al.* Quantification of latent tissue reservoirs and total body viral load in HIV-1 infection. *Nature* **387**, 183–188 (1997).
9. Chun, T.-W. *et al.* In vivo fate of HIV-1-infected T cells: Quantitative analysis of the transition to stable latency. *Nat. Med.* **1**, 1284–1290 (1995).
10. Chun, T. W. Presence of an inducible HIV-1 latent reservoir during highly active antiretroviral therapy. *Proc Natl Acad Sci USA* **94**, (1997).
11. Lee, G. Q. *et al.* Clonal expansion of genome-intact HIV-1 in functionally polarized Th1 $CD4^+$ T cells. *J. Clin. Invest.* **127**, 2689–2696 (2017).

12. Ho, Y. C. Replication-competent noninduced proviruses in the latent reservoir increase barrier to HIV-1 cure. *Cell* **155**, (2013).
13. Finzi, D. *et al.* Identification of a Reservoir for HIV-1 in Patients on Highly Active Antiretroviral Therapy. *Science* **278**, 1295–1300 (1997).
14. Charre, C., Merad, Y. & Avettand-Fenoel, V. HIV-1 reservoir landscape of post-treatment control. *Curr. Opin. HIV AIDS* https://doi.org/10.1097/COH.0000000000000891 (2024) doi:10.1097/COH.0000000000000891.
15. Sáez-Cirión, A. *et al.* Post-treatment HIV-1 controllers with a long-term virological remission after the interruption of early initiated antiretroviral therapy ANRS VISCONTI Study. *PLoS Pathog.* **9**, e1003211 (2013).
16. Gunst, J. D. *et al.* Time to HIV viral rebound and frequency of post-treatment control after analytical interruption of antiretroviral therapy: an individual data-based meta-analysis of 24 prospective studies. *Nat. Commun.* **16**, 906 (2025).
17. Namazi, G. *et al.* The Control of HIV After Antiretroviral Medication Pause (CHAMP) Study: Posttreatment Controllers Identified From 14 Clinical Studies. *J. Infect. Dis.* **218**, 1954–1963 (2018).
18. Murray, J. M. Latent HIV dynamics and implications for sustained viral suppression in the absence of antiretroviral therapy. *J. Virus Erad.* **4**, 91–98 (2018).
19. Passaes, C. *et al.* Early antiretroviral therapy favors post-treatment SIV control associated with the expansion of enhanced memory CD8+ T-cells. *Nat. Commun.* **15**, 178 (2024).
20. Daly, M. B. *et al.* SHIV remission in macaques with early treatment initiation and ultra long-lasting antiviral activity. *Nat. Commun.* **15**, 10550 (2024).
21. Hocqueloux, L. *et al.* Long-term antiretroviral therapy initiated during primary HIV-1 infection is key to achieving both low HIV reservoirs and normal T cell counts. *J. Antimicrob. Chemother.* **68**, 1169–1178 (2013).
22. Colby, D. J. Rapid HIV RNA rebound after antiretroviral treatment interruption in persons durably suppressed in Fiebig I acute HIV infection. *Nat Med* **24**, (2018).
23. Assoumou, L. A low HIV-DNA level in peripheral blood mononuclear cells at antiretroviral treatment interruption predicts a higher probability of maintaining viral control. *AIDS* **29**, (2015).
24. Saez-Cirion, A. HIV controllers exhibit potent CD8 T cell capacity to suppress HIV infection ex vivo and peculiar cytotoxic T lymphocyte activation phenotype. *Proc Natl Acad Sci USA* **104**, (2007).
25. Etemad, B. HIV post-treatment controllers have distinct immunological and virological features. *Proc Natl Acad Sci USA* **120**, (2023).
26. Hurst, J. Immunological biomarkers predict HIV-1 viral rebound after treatment interruption. *Nat Commun* **6**, (2015).
27. Avettand-Fenoel, V. *et al.* HIV-DNA in rectal cells is well correlated with HIV-DNA in blood in different groups of patients, including long-term non-progressors. *AIDS Lond. Engl.* **22**, 1880–1882 (2008).
28. Rose, R. *et al.* HIV Maintains an Evolving and Dispersed Population in Multiple Tissues during Suppressive Combined Antiretroviral Therapy in Individuals with Cancer. *J. Virol.* **90**, 8984–8993 (2016).
29. Lamers, S. L. *et al.* HIV DNA Is Frequently Present within Pathologic Tissues Evaluated at Autopsy from Combined Antiretroviral Therapy-Treated Patients with Undetectable Viral Loads. *J. Virol.* **90**, 8968–8983 (2016).
30. De Scheerder, M.-A. *et al.* HIV Rebound Is Predominantly Fueled by Genetically Identical Viral Expansions from Diverse Reservoirs. *Cell Host Microbe* **26**, 347-358.e7 (2019).

31. Chaillon, A. *et al.* HIV persists throughout deep tissues with repopulation from multiple anatomical sources. *J. Clin. Invest.* **130**, 1699–1712 (2020).
32. Dufour, C. *et al.* Near full-length HIV sequencing in multiple tissues collected postmortem reveals shared clonal expansions across distinct reservoirs during ART. *Cell Rep.* **42**, 113053 (2023).
33. Ganusov, V. V. & De Boer, R. J. Do most lymphocytes in humans really reside in the gut? *Trends Immunol.* **28**, 514–518 (2007).
34. Chun, T.-W. *et al.* Persistence of HIV in Gut-Associated Lymphoid Tissue despite Long-Term Antiretroviral Therapy. *J. Infect. Dis.* **197**, 714–720 (2008).
35. Yukl, S. A. *et al.* The Distribution of HIV DNA and RNA in Cell Subsets Differs in Gut and Blood of HIV-Positive Patients on ART: Implications for Viral Persistence. *J. Infect. Dis.* **208**, 1212–1220 (2013).
36. Estes, J. D. *et al.* Defining total-body AIDS-virus burden with implications for curative strategies. *Nat. Med.* **23**, 1271–1276 (2017).
37. Leyre, L. *et al.* Abundant HIV-infected cells in blood and tissues are rapidly cleared upon ART initiation during acute HIV infection. *Sci. Transl. Med.* **12**, eaav3491 (2020).
38. Benlhassan-Chahour, K. Kinetics of lymphocyte proliferation during primary immune response in macaques infected with pathogenic simian immunodeficiency virus SIVmac251: preliminary report of the effect of early antiviral therapy. *J Virol* **77**, (2003).
39. Fray, E. J. et al. Antiretroviral therapy reveals triphasic decay of intact SIV genomes and persistence of ancestral variants. Cell Host Microbe. 0, https://doi.org/10.1016/j.chom.2023.01.016 (2023).
40. Mannioui, A. Dynamics of viral replication in blood and lymphoid tissues during SIVmac251 infection of macaques. *Retrovirology* **6**, (2009).
41. Policicchio, B. B., Pandrea, I. & Apetrei, C. Animal models for HIV cure research. *Front Immunol* **7**, (2016).
42. Goulder, P. & Deeks, S. G. HIV control: Is getting there the same as staying there? *PLOS Pathog.* **14**, e1007222 (2018).
43. Mastrangelo, A. *et al.* Anti-HIV antibodies are representative of the latent reservoir but do not correlate with viral control in people with long-lasting virological suppression undergoing analytical treatment interruption (APACHE study). *J. Antimicrob. Chemother.* **76**, 1646–1648 (2021).
44. Jambo, K. C. *et al.* Small alveolar macrophages are infected preferentially by HIV and exhibit impaired phagocytic function. *Mucosal Immunol.* **7**, 1116–1126 (2014).
45. Clarke, J. R. *et al.* HIV-1 proviral DNA copy number in peripheral blood leucocytes and bronchoalveolar lavage cells of AIDS patients. *Clin. Exp. Immunol.* **96**, 182–186 (1994).
46. Costiniuk, C. T. *et al.* HIV persistence in mucosal CD4+ T cells within the lungs of adults receiving long-term suppressive antiretroviral therapy. *AIDS Lond. Engl.* **32**, 2279–2289 (2018).
47. Canaud, G. *et al.* The Kidney as a Reservoir for HIV-1 after Renal Transplantation. *J. Am. Soc. Nephrol.* **25**, 407–419 (2014).
48. Hughes, K. *et al.* HIV-1 infection of the kidney: mechanisms and implications. *AIDS* **35**, 359–367 (2021).
49. Baker, E. J., Hughes, K., Travieso, T., Klotman, M. E. & Blasi, M. Establishment, Persistence, and Reactivation of Latent HIV-1 Infection in Renal Epithelial Cells. *J. Virol.* **96**, e00624-22 (2022).
50. Trémeaux, P. *et al.* In-Depth Characterization of Full-Length Archived Viral Genomes after Nine Years of Posttreatment HIV Control. *Microbiol. Spectr.* **11**, e0326722 (2023).

51. Abrahams, M.-R. *et al.* The replication-competent HIV-1 latent reservoir is primarily established near the time of therapy initiation. *Sci. Transl. Med.* **11**, eaaw5589 (2019).
52. Lichterfeld, M., Gao, C. & Yu, X. G. An ordeal that does not heal: understanding barriers to a cure for HIV-1 infection. *Trends Immunol.* **43**, 608–616 (2022).
53. Cadena, A. M. *et al.* Persistence of viral RNA in lymph nodes in ART-suppressed SIV/SHIV-infected Rhesus Macaques. *Nat. Commun.* **12**, 1474 (2021).
54. Solis-Leal, A. *et al.* Lymphoid tissues contribute to plasma viral clonotypes early after antiretroviral therapy interruption in SIV-infected rhesus macaques. *Sci. Transl. Med.* **15**, eadi9867 (2023).
55. Passaes, C. Optimal maturation of the SIV-specific CD8+ T cell response after primary infection is associated with natural control of SIV: ANRS SIC study. *Cell Rep* **32**, (2020).
56. Harper, J. IL-21 and IFNalpha therapy rescues terminally differentiated NK cells and limits SIV reservoir in ART-treated macaques. *Nat Commun* **12**, (2021).
57. Climent, N. *et al.* Immunological and virological findings in a patient with exceptional post-treatment control: a case report. *Lancet HIV* **10**, e42–e51 (2023).
58. Essat, A. *et al.* A genetic fingerprint associated with durable HIV remission after interruption of antiretroviral treatment: ANRS VISCONTI/PRIMO. *Med* 100670 (2025) doi:10.1016/j.medj.2025.100670.
59. Armani-Tourret, M. *et al.* Immune targeting of HIV-1 reservoir cells: a path to elimination strategies and cure. *Nat. Rev. Microbiol.* **22**, 328–344 (2024).
60. Lian, X. *et al.* Progressive transformation of the HIV-1 reservoir cell profile over two decades of antiviral therapy. *Cell Host Microbe* **31**, 83-96.e5 (2023).
61. Li, J. Z. *et al.* Predictors of HIV rebound differ by timing of antiretroviral therapy initiation. *JCI Insight* **9**, e173864 (2024).
62. Mesquita, F. S., Li, Y. & Li, J. Z. Viral and immune predictors of HIV posttreatment control. *Curr. Opin. HIV AIDS* **20**, 54 (2025).
63. Giron, L. B., Pasternak, A. O. & Abdel-Mohsen, M. Soluble markers of viral rebound and post-treatment HIV control. *Curr. Opin. HIV AIDS* 10.1097/COH.0000000000000889 doi:10.1097/COH.0000000000000889.
64. Wedrychowski, A. Transcriptomic signatures of human immunodeficiency virus post-treatment control. *J Virol* **97**, (2022).
65. Hofmann-Lehmann, R. Sensitive and robust one-tube real-time reverse transcriptase-polymerase chain reaction to quantify SIV RNA load: comparison of one- versus two-enzyme systems. *AIDS Res Hum Retroviruses* **16**, (2000).
66. Bruner, K. M. A quantitative approach for measuring the reservoir of latent HIV-1 proviruses. *Nature* **566**, (2019).
67. Bender, A. M. *et al.* The Landscape of Persistent Viral Genomes in ART-Treated SIV, SHIV, and HIV-2 Infections. *Cell Host Microbe* **26**, 73-85.e4 (2019).
68. Policicchio, B. B. *et al.* Dynamics of Simian Immunodeficiency Virus Two-Long-Terminal-Repeat Circles in the Presence and Absence of CD8+ Cells. *J. Virol.* **92**, e02100-17 (2018).
69. Levy, C. N. *et al.* A highly multiplexed droplet digital PCR assay to measure the intact HIV-1 proviral reservoir. *Cell Rep. Med.* **2**, 100243 (2021).
70. Cai, D. & Sun, Y. Reconstructing viral haplotypes using long reads. *Bioinforma. Oxf. Engl.* **38**, 2127–2134 (2022).
71. Pinzone, M. R. *et al.* Longitudinal HIV sequencing reveals reservoir expression leading to decay which is obscured by clonal expansion. *Nat. Commun.* **10**, 728 (2019).

72. Chaillon, A. *et al.* HIV persists throughout deep tissues with repopulation from multiple anatomical sources. *J. Clin. Invest.* **130**, 1699–1712.
73. Estimation of the number of nucleotide substitutions in the control region of mitochondrial DNA in humans and chimpanzees. *Mol. Biol. Evol.* https://doi.org/10.1093/oxfordjournals.molbev.a040023 (1993) doi:10.1093/oxfordjournals.molbev.a040023.
74. Nguyen, L.-T., Schmidt, H. A., von Haeseler, A. & Minh, B. Q. IQ-TREE: a fast and effective stochastic algorithm for estimating maximum-likelihood phylogenies. *Mol. Biol. Evol.* **32**, 268–274 (2015).
75. Sáez-Cirión, A., Shin, S. Y., Versmisse, P., Barré-Sinoussi, F. & Pancino, G. Ex vivo T cell–based HIV suppression assay to evaluate HIV-specific CD8+ T-cell responses. *Nat. Protoc.* **5**, 1033–1041 (2010).

Acknowledgments

This study was funded by MSDAvenir though a research grant to the ANRS-RHIVIERA consortium, and the ANRS | Emerging infectious diseases French agency. A.M. E.G. and M.F. were supported by ANRS. IDMIT was supported by ANR French agency under references ANR-11-INBS-0008 and ANR-10-EQPX-02-01. We thank animal care workers, in particular Sebastien Langlois, Benoit Delache, Clare-Maelle Fovet, Maxime Pottier, Jean-Marie Robert as well as Julie Morin, Laetitia Bossevot, Brice Targat, Wesley Gros, Marco Leonec for expert technical assistance and Isabelle Mangeot-Méderlé for helpful project management at IDMIT. FTC, DTG, and TDF were obtained from Gilead and ViiV Healthcare through the "*IAS Towards an HIV Cure"* common Material Transfer Agreement. The SIV1C cell line was kindly provided by François Villinger.

Author contributions

C.R., R.L.G, and A.S.C. designed the pVISCONTI program with the contribution of D.D., O.L., M.M.T., N.D.B and V.A.F. C.R. and V.A.F. designed the virological study of this program. C.R., R.L.G, A.S.C. and V.A.F. obtained funding. C.C, A.M, A.Mi and V.A.F. designed the experiments. C.C., A.M., E.G., D.D., C.P., A.Mi., M.F., N.D., V.M. and N.D.B. carried out the experiments. C.C., A.M., A.C., E.G., D.D., C.P., A.Mi, M.F., N.D., V.M., N.D.B., R.L.G, A.S.C. and V.A.F. analyzed the data. C.C., A.M., A.C., M.M.T., C.R., R.L.G, A.S.C. and V.A.F. interpreted the results. V.A.F.

supervised the study. C.C. and V.A.F. wrote the manuscript with assistance from A.M. All authors critically reviewed the manuscript and contributed to the final version.

Competing interests

C.C. honoraria and travel grants from MSD, ViiV Healthcare and Gilead Sciences for participation in educational programs and conferences. A.S.C. has received speaker fees from MSD, ViiV Healthcare, Gilead, Janssen. V.A.F. has received grants (to her institution) from ViiV Healthcare and honoraria and travel grants from ViiV Healthcare and Gilead Sciences for participation in educational programs and conferences. The other authors declare no competing interests.

FIGURE LEGENDS

Fig. 1| Study design and plasma viral load (pVL) kinetics.

a, Schematic representation of the pVISCONTI study design. b, pVL in post-treatment controllers (PTCs, shown in blue, n=11) and non-controllers (NCs, pink, n=11) before treatment initiation, during treatment, and after analytical treatment interruption (ATI). pVL kinetics of macaques treated 4 weeks post-infection are shown with dotted lines, while those treated 24 weeks post-infection are shown with solid lines. The time scale is presented in days relative to ATI. c, pVL in treated macaques without ATI (shown in purple, n=11). The time scale is presented in days relative to treatment intiation. d, pVL in never treated macaques (shown in grey, n=15). The time scale is presented in days relative to infection. e, pVL at the time of euthanasia in never treated macaques (n=15), NCs (n=11), PTCs (n=11) and treated macaques without ATI (n=11). Values represent individual animals and are shown with medians and interquartile ranges. Statistical significance was determined using the Kruskal-Wallis test: *P<0.05, **P<0.01, ***P<0.001; ****P<0.0001. Source data are provided as a Source Data file. Exact P values and sample sizes are provided in the first sheet of the Source data file.

Fig. 2| Kinetics of total SIV-DNA and unspliced cell-associated SIV RNA in blood and peripheral lymph nodes (PLN). a, Total SIV-DNA in blood CD4+T cells. b, SIV unspliced cell-associated RNA (caRNA) in Peripheral Blood Mononuclear Cells (PBMCs). c, Total SIV-DNA in PBMCs. d, Total SIV-DNA in peripheral lymph node (PLN) CD4+ T Cells. e, Total SIV-DNA in PLN. f, SIV unspliced caRNA in PLN. Kinetics are represented before treatment initiation (days post-infection [p.i.]), during antiretroviral treatment (days post-treatment initiation [post-TT], in grey), for blood and before analytical treatment interruption (100 weeks post-treatment initiation [pre-ATI], in grey), after ATI (days post-ATI), and at euthanasia for blood and PLN, in post-treatment controllers (PTCs, blue) and non-controllers (NCs, pink). Results below the limit of detection are represented by empty circles. Values represent individual animals (n=5 to 11 for each group depending on sampling during the pVISCONTI study phases, details are provided in Fig. S11). Exact euthanasia time points are provided in Table S1. Median are shown. Statistical significance between PTCs and NCs was assessed using the 2-sided Mann-Whitney U test: *P<0.05, **P<0.01, ***P<0.001; ****P<0.0001. Source data are provided as a Source Data file. Exact P values and sample sizes are provided in the first sheet of the Source data file.

Fig. 3| Total SIV-DNA at euthanasia. Total SIV-DNA levels assessed in PBMCs (light red), lymphoid tissues (light blue) and multiple sites of gut (light green) at the time of euthanasia. Necropsies of PTCs and NCs were conducted at least 6 months after analytical treatment interruption. Values for never-treated macaques until euthanasia are represented in grey (n=4 to 15), non post-treatment controllers (NCs) in pink (n=5-11), post-treatment controllers (PTCs) are indicated in blue (n=7-11) and treated macaques without ATI in purple (n=4-11). Each sample size depends on the type of sample and on the experimental phase of the study; details are provided in Figure S11. Results below the limit of detection are represented by empty circles. Medians are shown. Statistical significance was determined using the Kruskal–Wallis test: *P<0.05, **P<0.01, ***P<0.001; ****P<0.0001. Source data are provided as a Source Data file. Exact P values and sample sizes are provided in the first sheet of the Source data file.

Fig. 4| Unspliced cell-associated SIV RNA at euthanasia. Unspliced cell-associated SIV RNA levels assessed in PBMCs (light red), lymphoid tissues (light blue) and multiple sites of gut (light green) at the time of euthanasia. Values for never-treated macaques until euthanasia are represented in grey (n=4 to 15), non post-treatment controllers (NCs) in pink (n=5-11), post-treatment controllers (PTCs) in blue (n=7-11) and treated macaques without ATI in purple (n=4-11). Each sample size depends on the type of sample and on the experimental phase of the study; details are provided in Figure S11. Results below the limit of detection are represented by empty circles. Medians are shown. Statistical significance was determined using the Kruskal–Wallis test: *P<0.05, **P<0.01, ***P<0.001; **** P<0.0001. Source data are provided as a Source Data file. Exact P values and sample sizes are provided in the first sheet of the Source data file.

Fig. 5| Estimation of intact proviruses levels using the Intact Proviral DNA Assay (IPDA) in PBMCs and tissues at euthanasia. Individual values are shown with medians and interquartile ranges for untreated macaques (grey, n=4 to 15), non post-treatement controllers (NCs, pink, n=5 to 11), post-treatment controllers (PTCs, blue, n=9 to 11) and treated macaques without ATI (purple, n=5 to 11). Each sample size depends on the type of sample and on the experimental phase of the study; details are provided in Figure S11. Results below the limit of detection are represented by empty circles. Statistical significance was assessed using the Kruskal–Wallis test: *P<0.05, **P<0.01, ***P<0.001; **** P<0.0001. Source data are provided as a Source Data file. Exact P values and sample sizes are provided in the first sheet of the Source data file.

Fig. 6| Intact proviruses in peripheral lymph nodes before analytical treatment interruption (ATI, 100 weeks after treatment initiation) a, Kinetics of intact proviruses in peripheral lymph node (PLN) prior to ATI and at the time of euthanasia according to post-treatment control (PTC) status and compared to treated macaques without ATI (purple) and never treatement macaques (grey). b, Correlation between pre-ATI intact proviruses in PLN and the post-ATI cumulative pVL (area under the curve [AUC], including all pVL measurements up to 6 months post-ATI). c, Correlation between pre-ATI intact proviruses in PLN

and the pVL assessed at the time of euthanasia. d, CD8+ T cell-mediated SIV-suppressive activity (log p27 decrease) according to PTC status in PLN prior to ATI. e, Correlation between SIV-suppressive activity of CD8+ T cells (log p27 decrease) and intact proviruses in PLN prior to ATI. For all panels, intact proviruses are quantified in disrupted cells obtained from both axillary and inguinal lymph nodes. Non post-treatment controllers (NCs) are represented in pink and post-treatment controllers (PTCs) in blue. In panels, a (pre-ATI), d, individual values for each macaque are shown with medians and interquartile ranges for NCs (a, n=11; d, n=10) and PTCs (a, n=10; d, n=7). Statistical significance was determined using 2-sided Mann-Whitney U test. In a, at the time of euthanasia individual values are shown with medians and interquartile ranges for untreated macaques (grey, n=4), NCs (n=5), PTCs (n=9) and treated macaques without ATI (purple, n=8). Statistical significance was determined using the Kruskal-Wallis test. In a, results below the limit of detection are represented by empty circles. In panels, b, c, e, non-parametric two-sided spearman correlation with 95% confidence interval was used for statistical analysis. *P<0.05, **P<0.01, ***P<0.001; ****P<0.0001. Each sample size depends on the type of sample and on the experimental phase of the study; details are provided in Figure S11. Source data are provided as a Source Data file. Exact P values and sample sizes are provided in the first sheet of the Source data file.

Fig. 7| Intact proviruses in PBMCs and blood-derived CD4+ T cells 7 days after ATI before rebound.

a, Kinetics of intact proviruses in PBMCs. Kinetics are represented before analytical treatment interruption (100 weeks post-treatment initiation [pre-ATI]), 7 days (D7) after ATI, and at euthanasia, in post-treatment controllers (PTCs, blue, n=11) and non post-treatment controllers (NCs, pink, n=11). At euthanasia, never treated macaques are represented in grey (n=13) and macaques under treatment without ATI are represented in purple (n=11). b, Intact proviruses in blood-derived CD4+ T cells D7 post-ATI according to PTC status (NCs, n=11; PTCs, n=10). c, Plasma viral load D7 post-ATI (NCs (pink, n=11) and PTCs (blue, n=11)). Values represent individual animals and are shown with medians and interquartile ranges. Statistical significance was assessed using the 2-sided Wilcoxon matched-pairs signed rank test for

comparisons within the same group at different time points, the two-sided Mann-Whitney U test for comparisons between two independent groups, or the Kruskal-Wallis test for comparisons involving more than two independent groups, particularly at euthanasia. In a, results below the limit of detection are represented by empty circles. d, Correlation between the pool of intact proviruses 7 days post-ATI in PBMCs and the cumulative plasma viral load after ATI (area under the curve [AUC], including all pVL measurements up to 6 months post-ATI). e, Correlation between the pool of intact proviruses in blood-derived CD4+ T cells D7 post-ATI and the cumulative plasma viral load after ATI. f, Correlation between the pool of intact proviruses 7 days post-ATI in PBMCs and and the pVL assessed at euthanasia. g, Correlation between the pool of intact proviruses in blood-derived CD4+ T cells D7 post-ATI and the pVL assessed at euthanasia. h, Correlation between the pool of intact proviruses in PLN before ATI and in PBMCs D7 post-ATI. i, Correlation between the pool of intact proviruses in PLN before ATI and in blood-derived CD4+ T cells D7 post-ATI. Non-parametric two-sided spearman correlation with 95% confidence interval was used for statistical analysis. *P<0.05, **P<0.01, ***P<0.001; ****P<0.0001, ns: non-significant. Source data are provided as a Source Data file. Exact P values and sample sizes are provided in the first sheet of the Source data file.

Fig. 8| Immune features associated with reservoir virological parameters measured at the end of the study. Heatmaps show spearman correlation coefficients between immune parameters and virological features of the SIV reservoir assessed at euthanasia across multiple tissues. Virological measures are grouped as Size (total SIV DNA, orange), Transcriptional activity (unspliced caRNA, pink), and Intactness (intact SIV DNA, purple). a, Humoral specific responses and CD8+ T cells functional readouts: post-ATI magnitude of anti-gp140 SIV IgG levels; $CD8^+$ T-cell SIV-suppressive activity (log_{10} p27 decrease) measured in PLN before ATI; magnitude (AUC) of $CD8^+$ T-cell SIV-suppressive activity measured in PBMCs after ATI; and frequencies of SIV-specific $CD8^+$ T cells producing one or four cytokines (IFN-γ, TNF-α, IL-2, CD107a) in blood at euthanasia. b, Phenotypic markers of $CD8^+$ T cells: proliferation defined by intracellular $Ki67^+$ expression, assessed in CD8+ or central memory (CM) CD8+ T cells in PLN and blood at indicated pre- and

post-ATI time points; stem-like or less-differentiated phenotype defined by $TCF1^+$ (self-renewal capacity), $CCR7^+$ (lymphoid recirculation capacity), and $PD\text{-}1^-$ (preserved functional capacity) memory $CD8^+$ T cells in the spleen at euthanasia; differentiation defined by effector $CD8^+$ T-cell subset assessed in blood after ATI; and activation of CD8+ T-cell defined by surface $CD38^+HLA\text{-}DR^+$ expression in PLN at euthanasia. Blue indicates negative and red positive correlations; color intensity reflects correlation strength (spearman coefficient). Asterisks denote statistical significance (two-sided test): P<0.05, *P<0.01, **P<0.001, ***P<0.0001. Source data are provided as a Source Data file. Exact P values and sample sizes are provided in the first sheet of the Source data file.

Fig. 9| Genetic divergence between intact proviral genomes at euthanasia and genomes of inoculum and circulating viruses at primary infection according to control post-treatment. a, Pairwise genetic distances between the inoculum and SIV RNA Near Full Length (NFL) genome from circulating viruses at different timepoints (indicated by a blue line), as well as proviruses at euthanasia (SIV DNA NFL genome, indicated by a red line). b, Pairwise genetic distances between sequences of viruses circulating at the time of primary infection to those of circulating viruses at different timepoints (SIV RNA NFL genome, indicated by blue line) and to proviruses at euthanasia (SIV DNA NFL genome indicated by red line). Pairwise genetic distances are shown for PTCs (n=1 to 5, early-treated macaques shown in empty blue circles, late-treated macaques shown full blue circles) and NCs (n=2 to 5, early-treated macaques shown in empty pink circles , late-treated macaques shown in full pink circles) with medians and interquartile ranges. Statistical significance was determined using the 2-sided Mann-Whitney U test: *P<0.05, **P<0.01, ***P<0.001; ****P<0.0001. CLN cervical lymph nodes, MLN mesenteric lymph nodes. Source data are provided as a Source Data file. Exact P values and sample sizes are provided in the first sheet of the Source data file.

Fig. 10| Individual phylogenetic trees. Haplotype sequences were obtained via near-full-length SIV genome nanopore sequencing of 5 post-treatment controllers (PTCs: 3 early-treated and 2 late-treated

macaques, panel a) and 5 non-controllers (NCs: 2 early-treated and 3 late-treated macaques, panel b). Phylogenies were rooted using the inoculum sequence and inferred using a maximum likelihood approach with IQ-TREE, employing the general time-reversible substitution model. Node labels indicate Shimodaira–Hasegawa approximate likelihood ratio test (SH-aLRT) support values (1000 replicates) shown only when >90%. Blue boxes highlight monophyletic clusters supported by ≥90% bootstrap and divergent from the inoculum and pre-ART circulating viral genomes. Blood plasma represent RNA near full length (NFL) genome from circulating viruses whereas the others compartments represent proviral NFL genome. Sites sampled at euthanasia are highlighted in blue in the legend. Scale bars are shown below each individual phylogenetic tree and denotes the number of nucleotide substitutions per site.

Editor's Summary

Using a non-human primate model, the authors show that SIV post-treatment control is associated with fewer intact proviruses in lymph nodes before treatment interruption, linked to stronger SIV-suppressive activity of CD8 T cells.

Peer review information: *Nature Communications* thanks Ole Søgaard, who co-reviewed with Katie Fisher and the other, anonymous, reviewer(s) for their contribution to the peer review of this work. A peer review file is available.

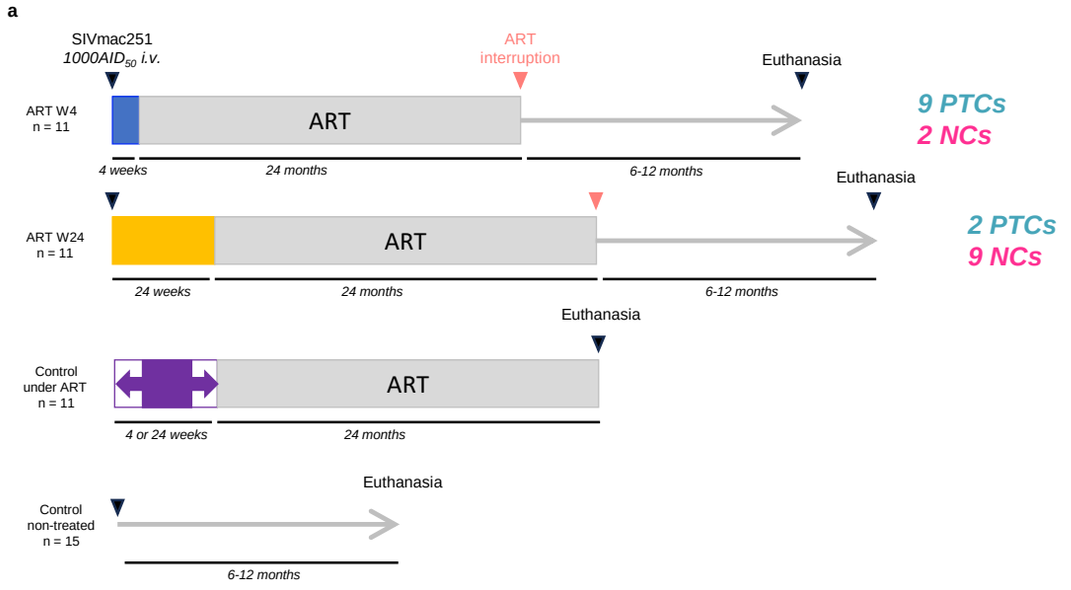
a
SIVmac251
1000AID50 i.v.
ART interruption
Euthanasia
ART W4
n = 11
ART
9 PTCs
2 NCs
4 weeks
24 months
6-12 months
Euthanasia
ART W24
n = 11
ART
2 PTCs
9 NCs
24 weeks
24 months
6-12 months
Euthanasia
Control
under ART
n = 11
ART
4 or 24 weeks
24 months
Euthanasia
Control
non-treated
n = 15
6-12 months

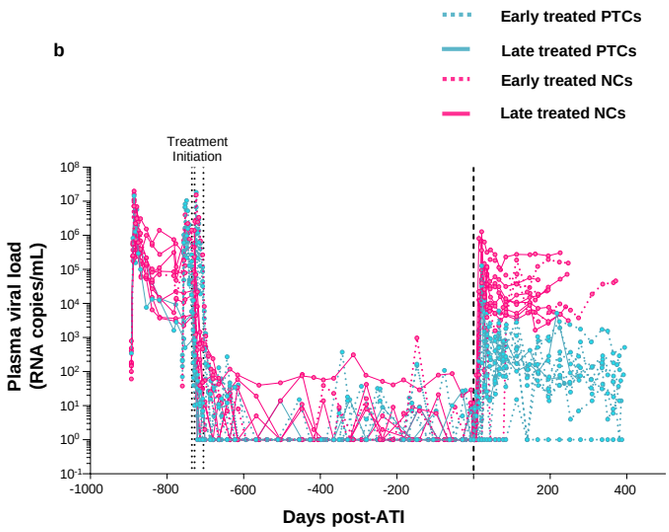
b
Early treated PTCs
Late treated PTCs
Early treated NCs
Late treated NCs
Treatment Initiation
Plasma viral load (RNA copies/mL)
Days post-ATI

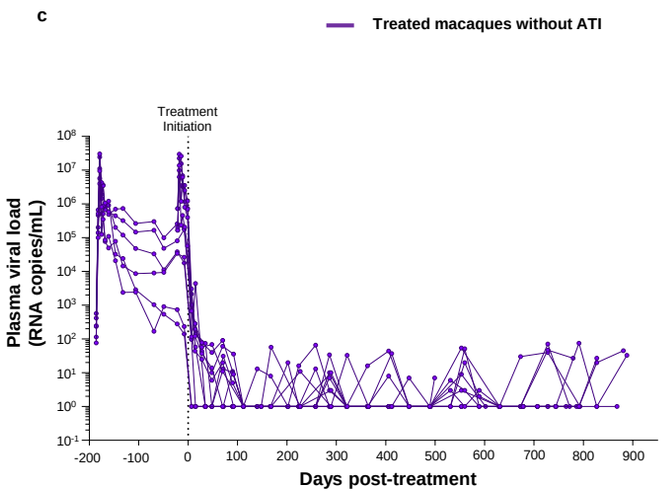
c
Treated macaques without ATI
Treatment Initiation
Plasma viral load (RNA copies/mL)
Days post-treatment

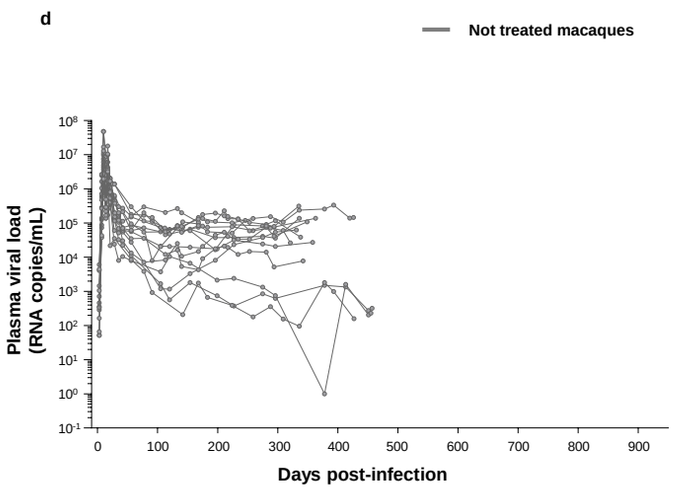
d
Not treated macaques
Plasma viral load (RNA copies/mL)
Days post-infection

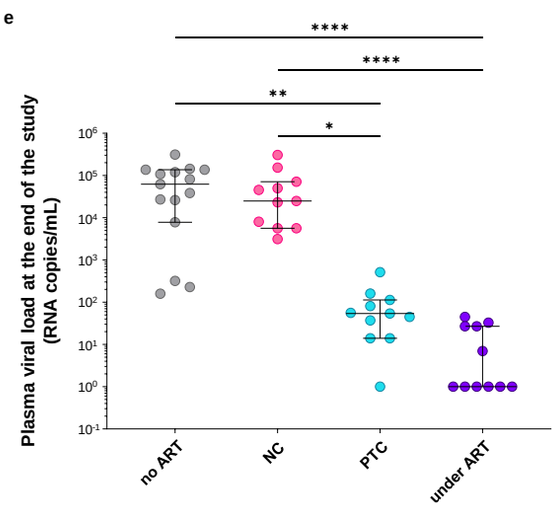
e
****
****
**
*
Plasma viral load at the end of the study (RNA copies/mL)
no ART
NC
PTC
under ART

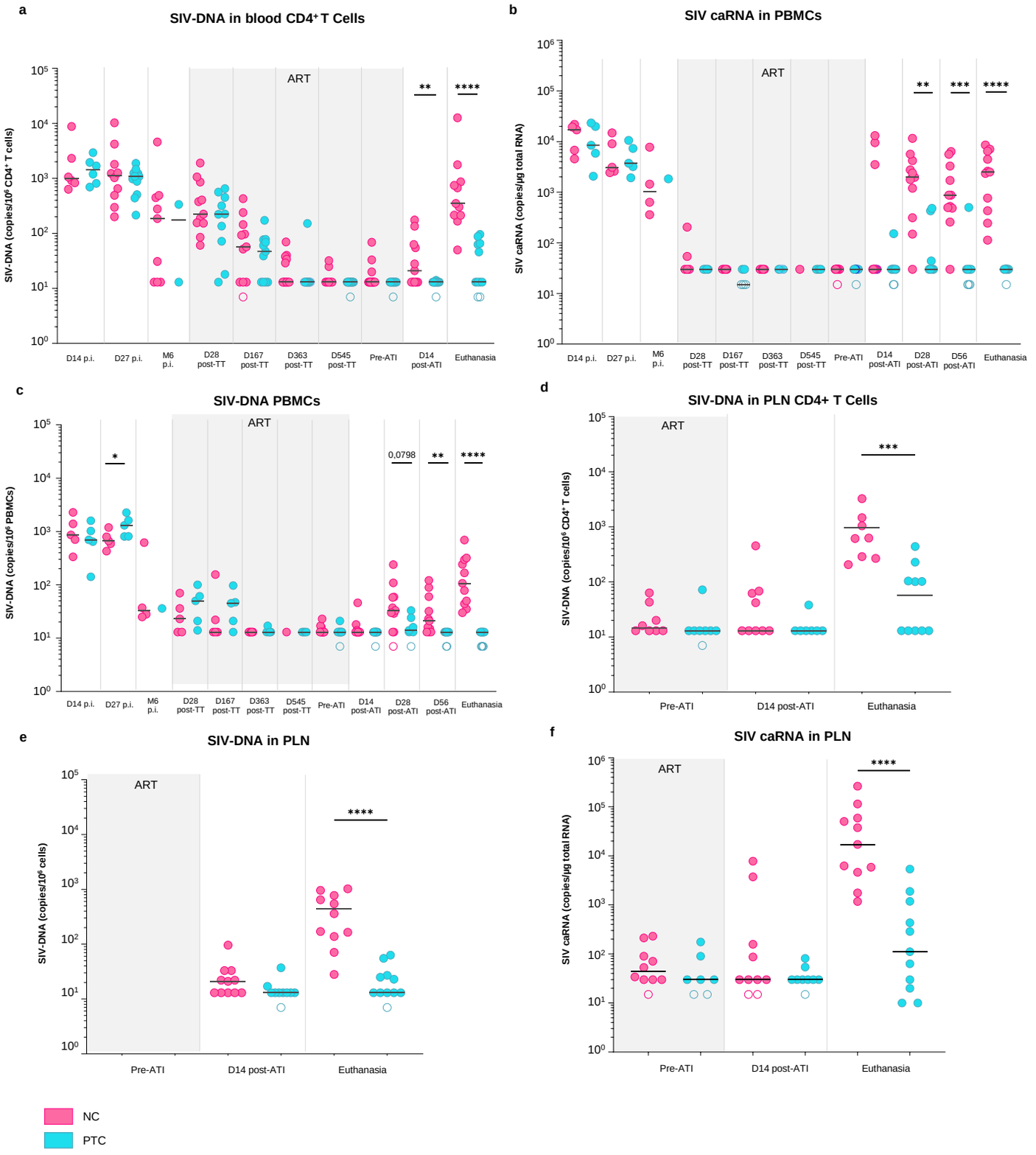
a
SIV-DNA in blood CD4+ T Cells
SIV-DNA (copies/10^6 CD4+ T cells)
ART
**
****
D14 p.i.
D27 p.i.
M6 p.i.
D28 post-TT
D167 post-TT
D363 post-TT
D545 post-TT
Pre-ATI
D14 post-ATI
Euthanasia
b
SIV caRNA in PBMCs
SIV caRNA (copies/µg total RNA)
ART
**
***
****
D28 post-ATI
D56 post-ATI
c
SIV-DNA PBMCs
SIV-DNA (copies/10^6 PBMCs)
*
0,0798
d
SIV-DNA in PLN CD4+ T Cells
e
SIV-DNA in PLN
f
SIV caRNA in PLN
Pre-ATI
D14 post-ATI
NC
PTC

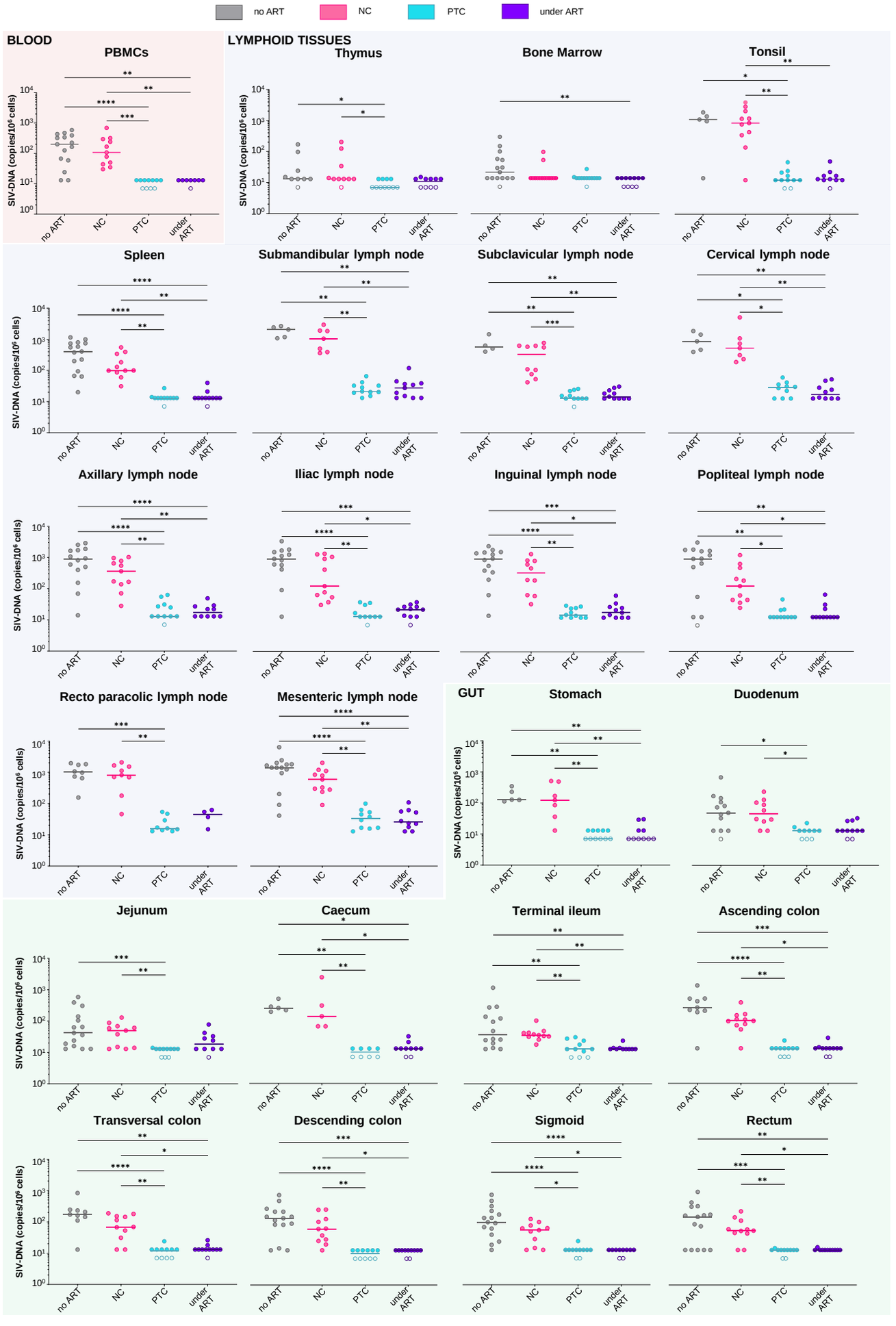
no ART
NC
PTC
under ART
BLOOD
PBMCs
LYMPHOID TISSUES
Thymus
Bone Marrow
Tonsil
Spleen
Submandibular lymph node
Subclavicular lymph node
Cervical lymph node
Axillary lymph node
Iliac lymph node
Inguinal lymph node
Popliteal lymph node
Recto paracolic lymph node
Mesenteric lymph node
GUT
Stomach
Duodenum
Jejunum
Caecum
Terminal ileum
Ascending colon
Transversal colon
Descending colon
Sigmoid
Rectum
SIV-DNA (copies/10⁶ cells)

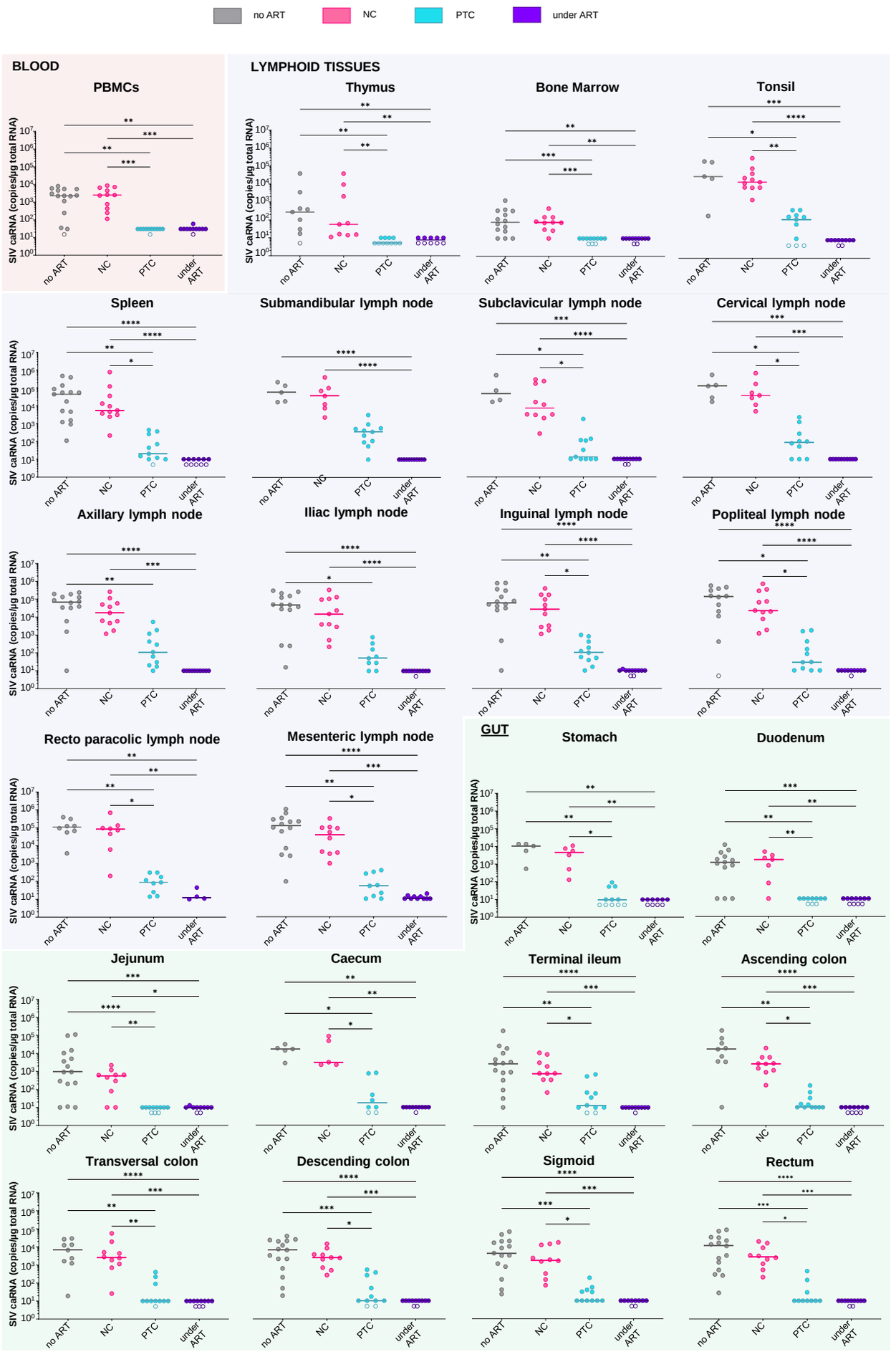
no ART
NC
PTC
under ART
BLOOD
PBMCs
LYMPHOID TISSUES
Thymus
Bone Marrow
Tonsil
Spleen
Submandibular lymph node
Subclavicular lymph node
Cervical lymph node
Axillary lymph node
Iliac lymph node
Inguinal lymph node
Popliteal lymph node
Recto paracolic lymph node
Mesenteric lymph node
GUT
Stomach
Duodenum
Jejunum
Caecum
Terminal ileum
Ascending colon
Transversal colon
Descending colon
Sigmoid
Rectum
SIV caRNA (copies/µg total RNA)

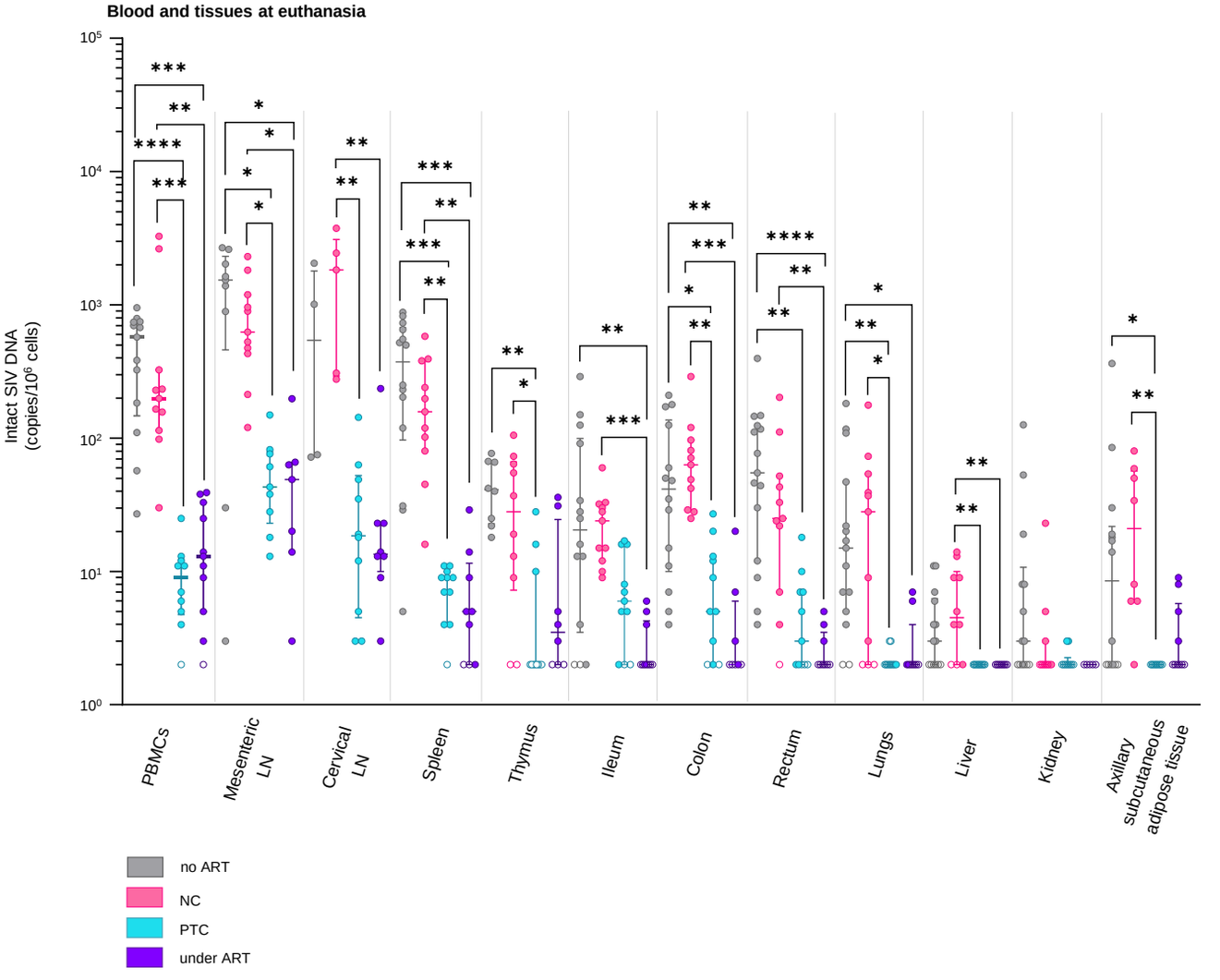
Blood and tissues at euthanasia
Intact SIV DNA (copies/10^6 cells)
10^5
10^4
10^3
10^2
10^1
10^0
PBMCs
Mesenteric LN
Cervical LN
Spleen
Thymus
Ileum
Colon
Rectum
Lungs
Liver
Kidney
Axillary subcutaneous adipose tissue
no ART
NC
PTC
under ART

Intact SIV DNA in PLN

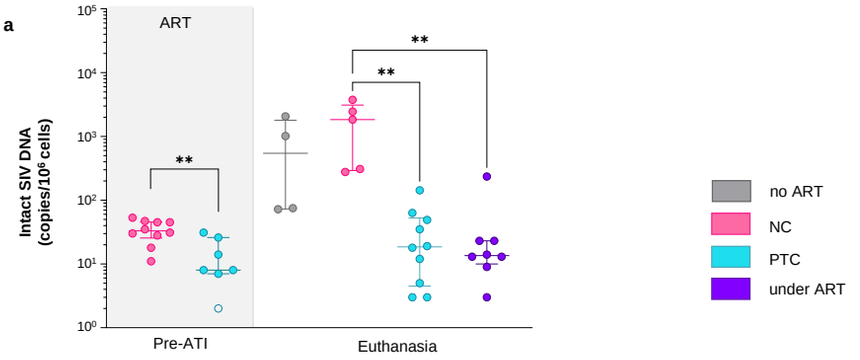

Association between pre-ATI intact SIV DNA in PLN and post-ATI replication

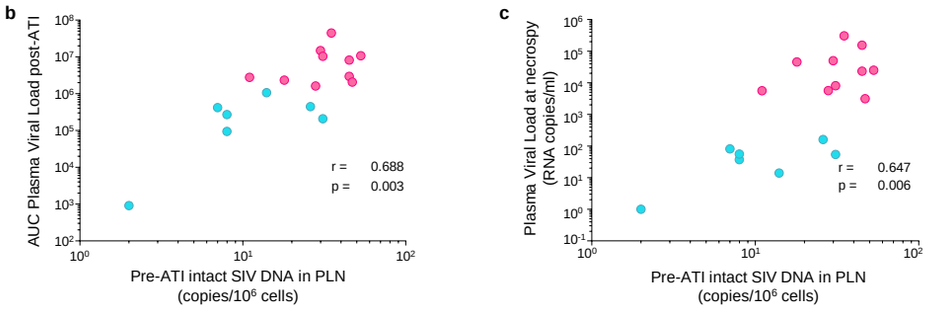

Association between pre-ATI intact SIV DNA in PLN and SIV-suppressive activity of CD8⁺ T cells

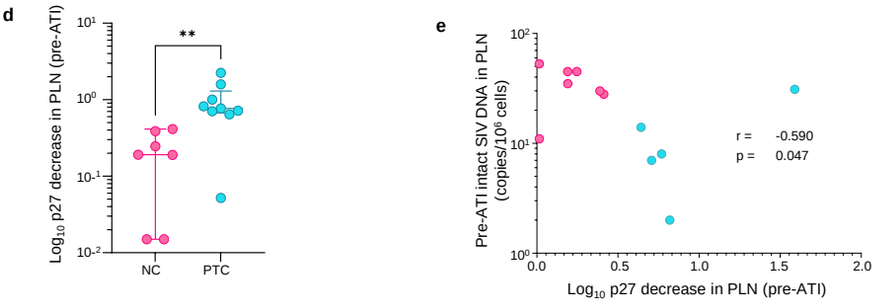

Intact proviruses in blood after ATI and before rebound

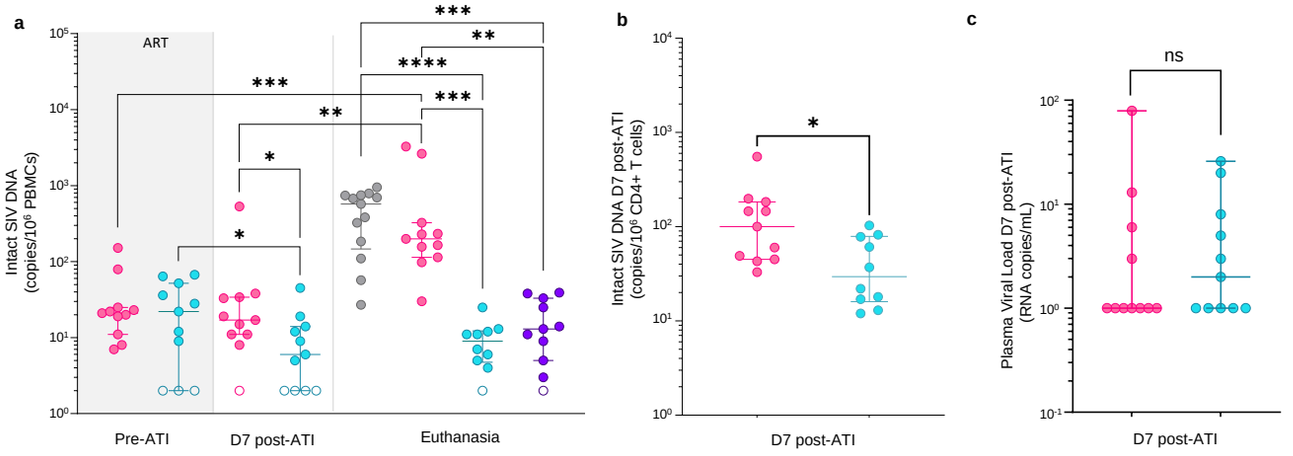

Association between pre-rebound intact SIV DNA in blood and post-ATI replication

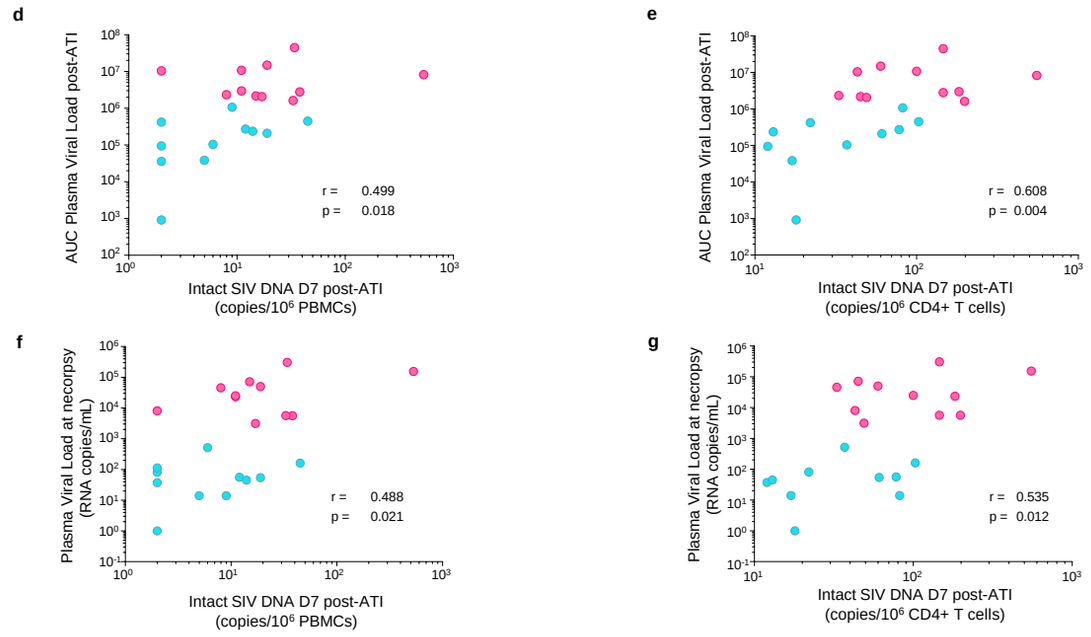

Association between pre-rebound intact SIV DNA in blood and pre-ATI intact SIV DNA in PLN

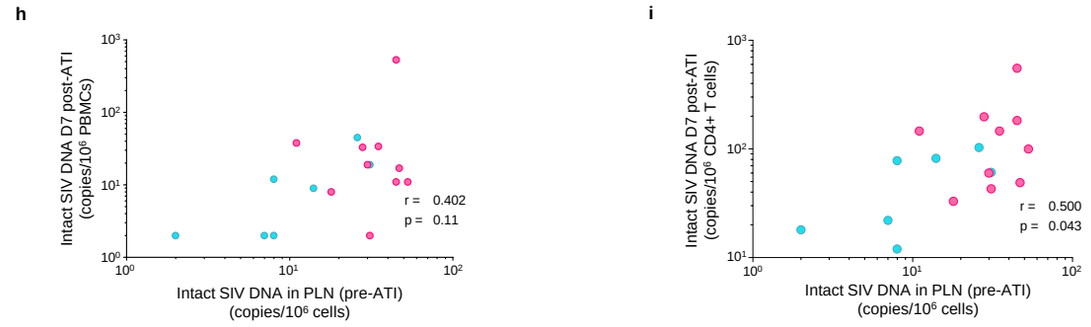

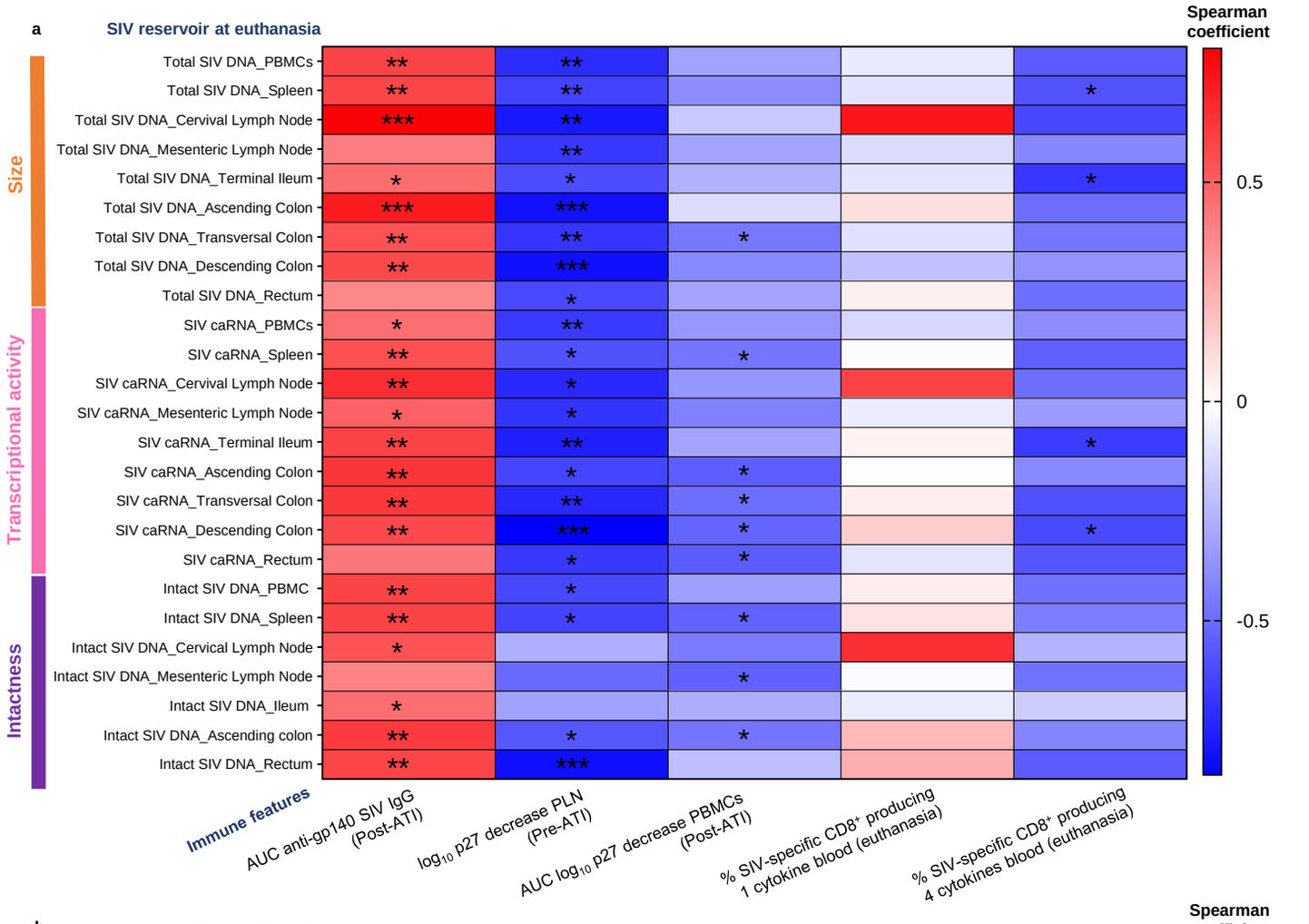
a
SIV reservoir at euthanasia
Spearman coefficient
0.5
0
-0.5
Size
Transcriptional activity
Intactness
Total SIV DNA_PBMCs
Total SIV DNA_Spleen
Total SIV DNA_Cervival Lymph Node
Total SIV DNA_Mesenteric Lymph Node
Total SIV DNA_Terminal Ileum
Total SIV DNA_Ascending Colon
Total SIV DNA_Transversal Colon
Total SIV DNA_Descending Colon
Total SIV DNA_Rectum
SIV caRNA_PBMCs
SIV caRNA_Spleen
SIV caRNA_Cervival Lymph Node
SIV caRNA_Mesenteric Lymph Node
SIV caRNA_Terminal Ileum
SIV caRNA_Ascending Colon
SIV caRNA_Transversal Colon
SIV caRNA_Descending Colon
SIV caRNA_Rectum
Intact SIV DNA_PBMC
Intact SIV DNA_Spleen
Intact SIV DNA_Cervical Lymph Node
Intact SIV DNA_Mesenteric Lymph Node
Intact SIV DNA_Ileum
Intact SIV DNA_Ascending colon
Intact SIV DNA_Rectum
Immune features
AUC anti-gp140 SIV IgG (Post-ATI)
log10 p27 decrease PLN (Pre-ATI)
AUC log10 p27 decrease PBMCs (Post-ATI)
% SIV-specific CD8+ producing 1 cytokine blood (euthanasia)
% SIV-specific CD8+ producing 4 cytokines blood (euthanasia)

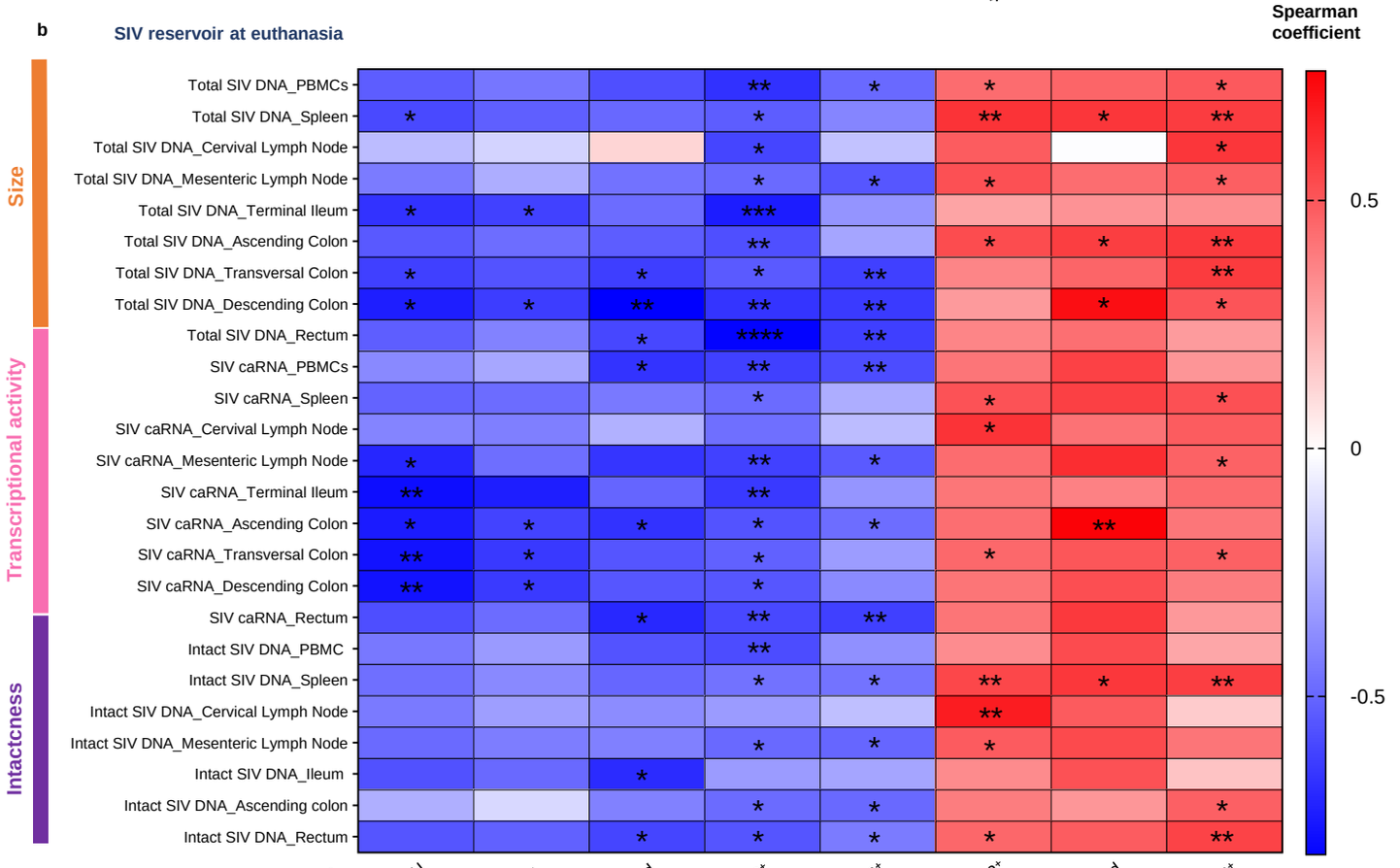
b
SIV reservoir at euthanasia
Spearman coefficient
0.5
0
-0.5
Size
Transcriptional activity
Intactcness
Total SIV DNA_PBMCs
Total SIV DNA_Spleen
Total SIV DNA_Cervival Lymph Node
Total SIV DNA_Mesenteric Lymph Node
Total SIV DNA_Terminal Ileum
Total SIV DNA_Ascending Colon
Total SIV DNA_Transversal Colon
Total SIV DNA_Descending Colon
Total SIV DNA_Rectum
SIV caRNA_PBMCs
SIV caRNA_Spleen
SIV caRNA_Cervival Lymph Node
SIV caRNA_Mesenteric Lymph Node
SIV caRNA_Terminal Ileum
SIV caRNA_Ascending Colon
SIV caRNA_Transversal Colon
SIV caRNA_Descending Colon
SIV caRNA_Rectum
Intact SIV DNA_PBMC
Intact SIV DNA_Spleen
Intact SIV DNA_Cervical Lymph Node
Intact SIV DNA_Mesenteric Lymph Node
Intact SIV DNA_Ileum
Intact SIV DNA_Ascending colon
Intact SIV DNA_Rectum
Immune features
Ki67+ % CD8+ PLN (D14 post-ATI)
Ki67+ % CM CD8+ PLN (D14 post-ATI)
Ki67+ % CM CD8+ blood (D28 post-ATI)
CCR7+% SIV-specific memory CD8+ spleen (euthanasia)
TCF1+ % SIV-specific memory CD8+ spleen (euthanasia)
PD1+ % SIV-specific memory CD8+ spleen (euthanasia)
Effector % CD8+ blood (D14 post-ATI)
CD38+ HLADR+ % CD8+ PLN (euthanasia)

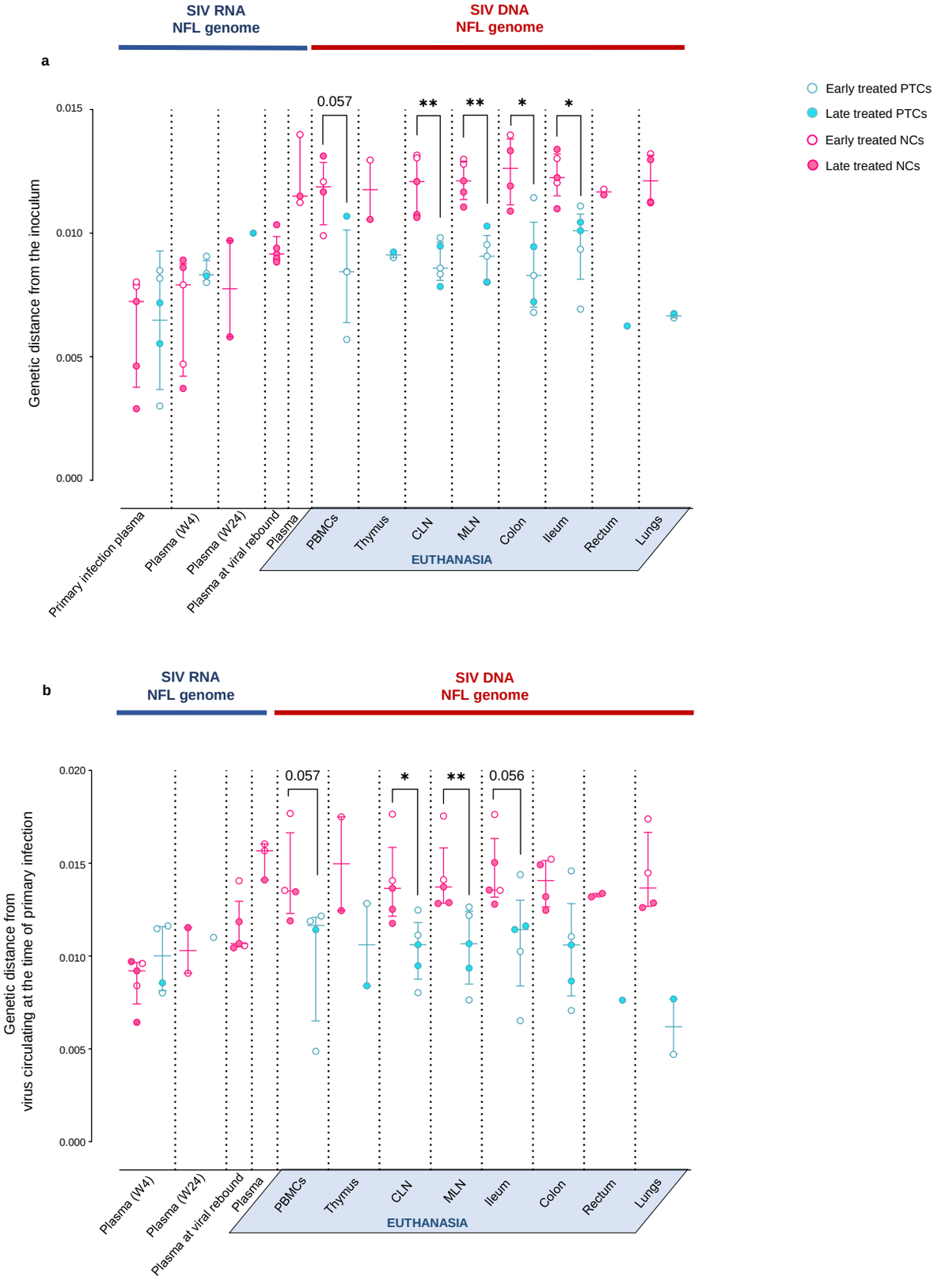
a
SIV RNA
NFL genome
SIV DNA
NFL genome
Genetic distance from the inoculum
0.015
0.010
0.005
0.000
0.057
**
**
*
*
Primary infection plasma
Plasma (W4)
Plasma (W24)
Plasma at viral rebound
Plasma
PBMCs
Thymus
CLN
MLN
Colon
Ileum
Rectum
Lungs
EUTHANASIA
Early treated PTCs
Late treated PTCs
Early treated NCs
Late treated NCs
b
SIV RNA
NFL genome
SIV DNA
NFL genome
Genetic distance from
virus circulating at the time of primary infection
0.020
0.015
0.010
0.005
0.000
0.057
*
**
0.056
Plasma (W4)
Plasma (W24)
Plasma at viral rebound
Plasma
PBMCs
Thymus
CLN
MLN
Ileum
Colon
Rectum
Lungs
EUTHANASIA

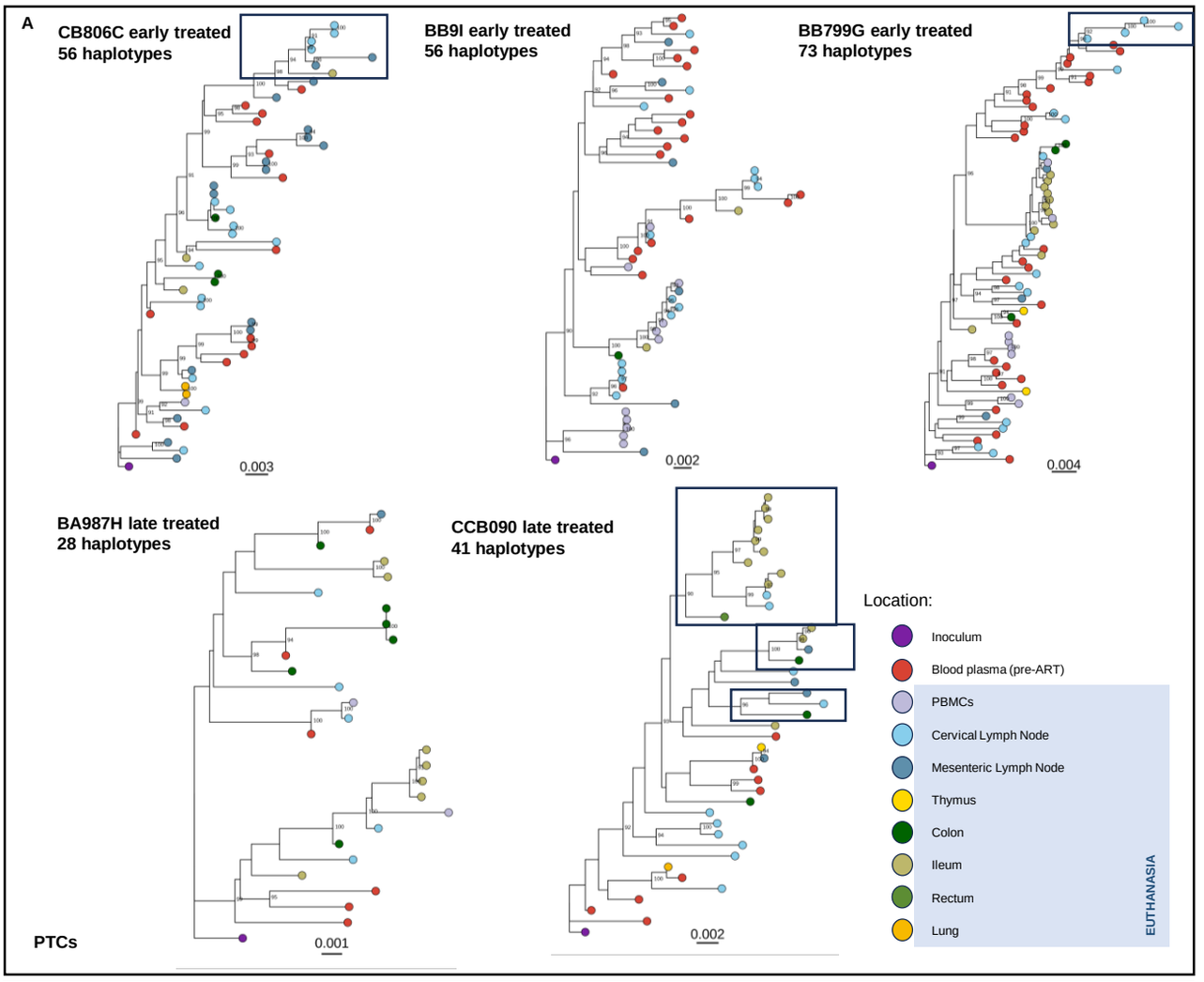
A
CB806C early treated
56 haplotypes
0.003
BB9I early treated
56 haplotypes
0.002
BB799G early treated
73 haplotypes
0.004
BA987H late treated
28 haplotypes
0.001
CCB090 late treated
41 haplotypes
0.002
PTCs
Location:
Inoculum
Blood plasma (pre-ART)
PBMCs
Cervical Lymph Node
Mesenteric Lymph Node
Thymus
Colon
Ileum
Rectum
Lung
EUTHANASIA

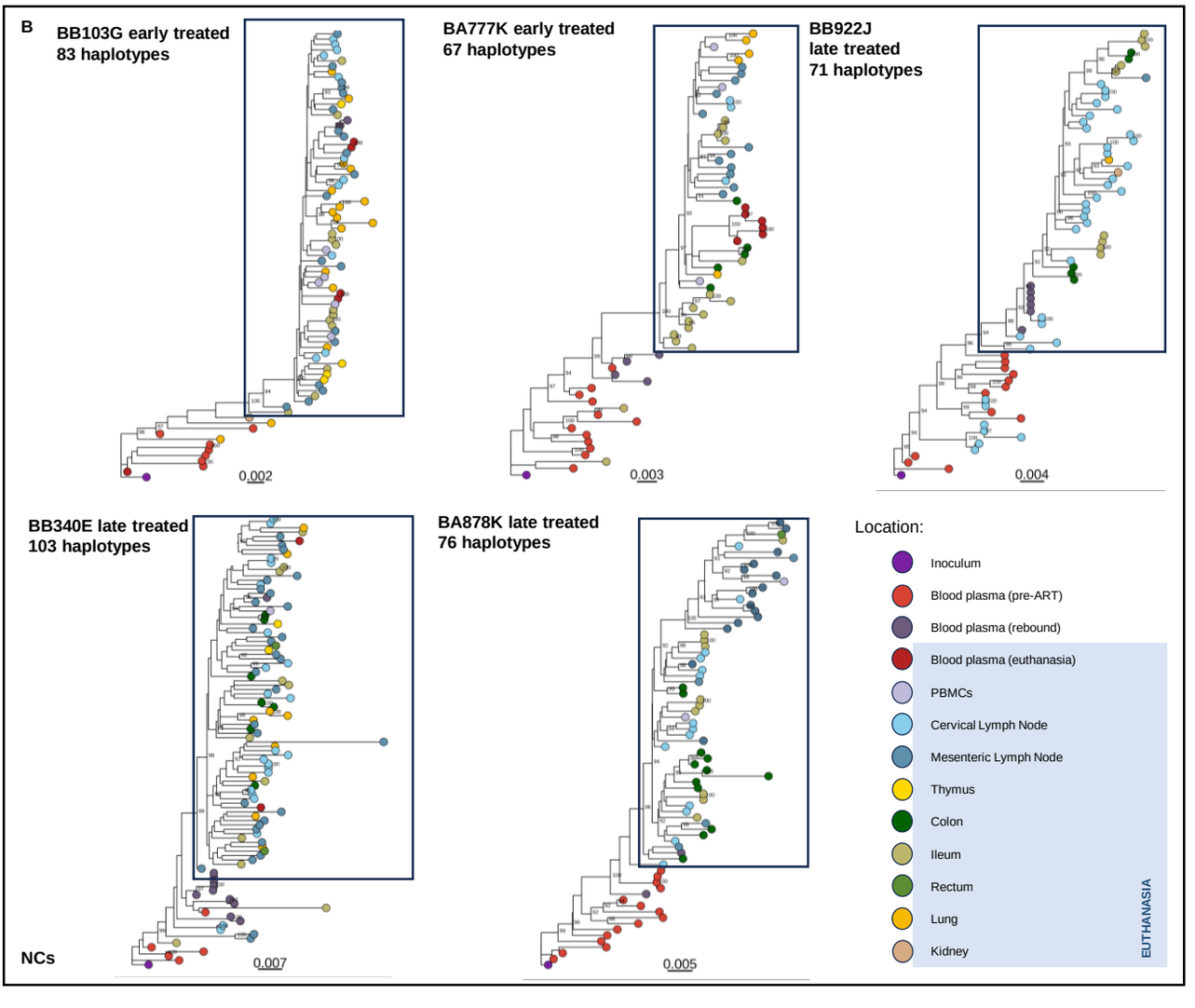
B
BB103G early treated
83 haplotypes
0.002
BA777K early treated
67 haplotypes
0.003
BB922J
late treated
71 haplotypes
0.004
BB340E late treated
103 haplotypes
0.007
BA878K late treated
76 haplotypes
0.005
NCs
Location:
Inoculum
Blood plasma (pre-ART)
Blood plasma (rebound)
Blood plasma (euthanasia)
PBMCs
Cervical Lymph Node
Mesenteric Lymph Node
Thymus
Colon
Ileum
Rectum
Lung
Kidney
EUTHANASIA